The impact of dissolved organic carbon and bacterial respiration on pCO_2 in experimental sea ice

Zhou, J.[1,2,3], M. Kotovitch[1,2], H. Kaartokallio[4], S. Moreau[5], J.-L. Tison[1], G. Kattner[6], G. Dieckmann[6], D.N. Thomas[4, 7], B. Delille[2]

[1] Laboratoire de glaciologie, DSTE, Université Libre de Bruxelles, Belgium

[2] Unité d'océanographie chimique, MARE, Université de Liège, Belgium

[3] Division of Earth and Ocean Sciences, Duke University, Durham, NC, USA

[4] Marine Research Centre, Finnish Environment Institute (SYKE), Helsinki, Finland

[5] Georges Lemaître Centre for Earth and Climate Research, Earth and Life Institute, Université catholique de Louvain, Louvain-la-Neuve, Belgium

[6] Alfred Wegener Institute Helmholtz Center for Polar and Marine Research, Bremerhaven, Germany

[7] School of Ocean Sciences, Bangor University, Menai Bridge, United Kingdom

Abstract

Previous observations have shown that the partial pressure of carbon dioxide (pCO_2) in sea ice brines is generally higher in Arctic sea ice compared to those from the Antarctic sea ice, especially in winter and early spring. We hypothesized that these differences result from the higher dissolved organic carbon (DOC) content in Arctic seawater: Higher concentrations of DOC in seawater would be reflected in a greater DOC incorporation into sea ice, enhancing bacterial respiration, which in turn would increase the pCO_2 in the ice. To verify this hypothesis, we performed an experiment using two series of mesocosms: one was filled with seawater (SW) and the other one with seawater with an addition of filtered humic-rich river water (SWR). The addition of river water increased the DOC concentration of the water from a median of 142 µmol L^{-1} in SW to 249 µmol L^{-1} in SWR. Sea ice was grown in these mesocosms under the same physical conditions over 19 days. Microalgae and protists were absent, and only bacterial activity has been detected. We measured the DOC concentration, bacterial respiration, total alkalinity and pCO_2 in sea ice and the underlying seawater, and we calculated the changes in dissolved inorganic carbon (DIC) in both media. We found that bacterial respiration in ice was

higher in SWR: median bacterial respiration was 25 nmol C L^{-1} h^{-1} compared to 10 nmol C L^{-1} h^{-1} in SW. pCO_2 in ice was also higher in SWR with a median of 430 ppm compared to 356 ppm in SW. However, the differences in pCO_2 were larger within the ice interiors than at the surfaces or the bottom layers of the ice, where exchanges at the air-ice and ice-water interfaces might have reduced the differences. In addition, we used a model to simulate the differences of pCO_2 and DIC based on bacterial respiration. The model simulations support the experimental findings and further suggest that bacterial growth efficiency in the ice might be 0.15-0.2. It is thus credible that the higher pCO_2 in Arctic sea ice brines compared with those from the Antarctic sea ice were due to an elevated bacterial respiration, sustained by higher riverine DOC loads. These conclusions should hold for locations and time frames when bacterial activity is relatively dominant compared to algal activity, considering our experimental conditions.

Highlights (85 characters per highlight)

- Brine concentration/dilution causes the largest temporal changes of pCO_2 in ice
- Elevated BR due to riverine DOC addition increases pCO_2 in sea ice
- Gas exchange and the buffer effect further affect the bacterial impact on pCO_2

Keywords (up to six)

Sea ice, dissolved organic matter, carbon dioxide, bacterial activity, gas exchange

1. Introduction

Sea ice is formed from the freezing of seawater and covers about 6 % of the Earth's ocean surface. It has a heterogeneous structure composed of a matrix of pure ice and brine inclusions. Although sea ice is currently assumed to be impermeable to gas exchange in large-scale climate models, theoretical considerations (Golden et al., 1998) and pioneer gas measurements (Gosink et al., 1976) indicate that sea ice may be permeable under specific conditions of ice temperature and salinity. Measurements of pCO_2 in sea ice and brines have been intensified in both the Arctic (Crabeck et al., 2014; Geilfus et al., 2012a; Miller et al., 2011a, 2011b) and the Southern Ocean (Delille, 2006; Delille et al., 2007; Geilfus et al., 2014). The motivation for these measurements is to better understand the role of sea ice in the carbon cycle, including its role

in air-sea exchange of CO_2, and the potential feedback effects between the changing ice cover, CO_2 fluxes, and climate change.

Current measurements indicate that sea ice may act as a source or a sink for atmospheric CO_2, depending on the interplay of four processes:

(i) Brine concentration and dilution are associated with changes in ice temperature. When cooling a sea ice sample, some of the liquid water of the brine freezes, reducing the brine volume and inclusions and increasing the concentration of the impurities in the brine – this is the so-called brine concentration. In contrast, when warming a sea ice sample, some of the pure ice melts, increasing the volume of the brine inclusion and decreasing the concentration of the impurities in brine – this is the so-called brine dilution (Hunke et al., 2011; Notz and Worster, 2009).

(ii) Biological activity, which includes the photosynthesis and respiration by organisms, respectively, consumes and produces CO_2 (e.g., Papadimitriou et al., 2007).

(iii) The precipitation and dilution of calcium carbonate, which produces and consumes CO_2, respectively (Dieckmann et al., 2010, 2008; Geilfus et al., 2013), effectively alters the CO_2 budget in the ice when sea ice is semi-permeable, and when the calcium carbonate precipitates remain in the ice while the generated CO_2 is rejected into the under-ice water (Delille et al., 2014; Rysgaard et al., 2007) or to the atmosphere (Geilfus et al., 2013; Loose et al., 2011).

(iv) Gas transport through sea ice is not yet well constrained, but it is commonly assumed that sea ice is permeable for gas transport when its brine volume fraction is above 5 % (Golden et al., 1998). Brine drainage – the intensity of which is estimated using Raleigh numbers – is thought to be a significant process for ice-water exchange (Notz and Worster, 2009), while gas bubble formation potentially plays an important role in air-ice exchange (Moreau et al., 2014; Zhou et al., 2013). The diffusion of CO_2 through sea ice also affects air-ice exchange, but seems to be much slower, i.e., less efficient than gas bubble transport (Kotovitch et al., submitted; Loose et al., 2014).

Previous studies indicate that, for a given brine temperature, the pCO_2 in sea ice brine in the Arctic Ocean (Geilfus et al., 2014, 2012a) was generally higher than that in the Southern Ocean (Delille et al., 2014; Geilfus et al., 2014), especially when the average ice temperature was below -4°C – which generally corresponds to the winter and early spring period (Figure 1). In this study, we hypothesized that the higher pCO_2 was associated to the more intense bacterial respiration in the Arctic sea ice, due to the large input of riverine particulate organic carbon

(POC) and dissolved organic carbon (DOC) in the Arctic Ocean (e.g., Dittmar and Kattner (2003); Hansell et al. (2009)). Ice temperature is unlikely to explain the Arctic-Antarctic discrepancies, because at a given temperature, the effect of brine concentration on pCO_2 is expected to be the same in both hemispheres. However, the impact of DOC availability on bacterial respiration and pCO_2 in sea ice has not yet been demonstrated by systematic DOC and POC measurements in parallel. Therefore we performed an indoor experiment using two series of mesocosms: One was filled with seawater (SW) and another with seawater and an addition of filtered river water (SWR) to simulate riverine DOC input. The objective of the present paper is to verify whether or not higher DOC concentrations in seawater, due to an addition of riverine DOC, induce larger DOC concentrations in sea ice, which in turn enhance bacterial respiration and pCO_2 in the ice.

2. Material and methods

2.1 Experimental setting, and sampling routine and initial conditions

The experimental setting and sampling routine has been described in Zhou et al. (2014). Briefly, we ran a 19-day experiment in the Arctic Environmental Test Basin facility of the Hamburg Ship Model Basin (www.hsva.de) from May to June 2012. We used 21 polyethylene experimental mesocosms each with a volume of 1.2 m^3. Eleven of the mesocosms were filled with 1000 L of seawater from the North Sea (referred here after as SW), and the remaining ten were filled with 900 L of seawater from the North Sea and 100 L of filtered river water collected at a peat-dominated catchment of the River Kiiminkijoki, in Finland (referred here after as SWR).

The addition of river water caused a significantly higher DOC concentration in the SWR mesocosms (paired t-test, $p<0.001$): Median salinity-normalized DOC concentrations were 140 µmol L^{-1} in SW and 251 µmol L^{-1} in SWR (salinity 30.9), with a standard deviation of 3 % in the SW mesocosms and 9 % in SWR. However, salinity-normalized dissolved organic nitrogen (DON) was not significantly different between both mesocosm series (median of 16 µmol L^{-1} in SW and 19 µmol L^{-1} in SWR), because its concentration in river and North Sea water were almost the same, and the standard deviation was relatively high (17 %) in both SW and SWR mesocosms. The carbonate chemistry was also not significantly different for both mesocosm series: median salinity-normalized total alkalinity was 2314 µmol kg^{-1} in SW and 2336 µmol kg^{-1} in SWR; median salinity-normalized dissolved inorganic carbon (DIC) were 2113 µmol kg^{-1} in SW and and 2161 µmol kg^{-1} in SWR; and median pCO_2 were 212 ppm in SW and 231

126 ppm in SWR, respectively. The salinities of the SWR mesocosms were adjusted to the SW
127 values by adding aquarium standard salt (Tropic Marin®). Nitrate (NO_3^-) and phosphate (PO_4^{3-}
128) concentrations were also adjusted to concentrations that would not limit bacterial growth in
129 both series of mesocosms, and that were representative of areas in both Arctic and Southern
130 Oceans (Zhou et al., 2014).

131 Ice was grown from day 0 to 14, during which the air temperature was maintained at -14 °C,
132 and then the air temperature was increased to -1 °C to trigger a decay phase. We collected ice,
133 brine and seawater at various occasions from day 0 to day 19 for the measurements of
134 temperature, salinity, DOC, inorganic nutrients, bacterial abundance, and bacterial activity
135 (Zhou et al., 2014), as well as pCO_2 and total alkalinity.

136 Because the physical constraints were similar for both the SW and SWR mesocosms, we
137 expected bacterial activity to be the only process affecting the difference of pCO_2 in both water
138 and ice. Median bacterial abundance was 922 cells L^{-1} in SW at the beginning of the experiment
139 and was not significantly different from the 972 cells L^{-1} in SWR. Protists and active
140 photoautotrophs were absent in the experiment (checked by microscopy and epifluorescence
141 microscopy, respectively). As a corollary, there was no autochthonous production of DOC and
142 our experiment focuses on the impact of the additional allochtonous DOC (added by the river
143 water) on bacterial respiration and pCO_2 in both water and ice. Although photoautotrophs were
144 absent in our experiments, we believe that it would not drastically affect the verification of the
145 hypothesis, because the largest observed difference of pCO_2 in brine corresponds to the lowest
146 ice temperature (Figure 1), which mostly correspond to the ice interior (over winter and early
147 spring) where algal activity is relatively limited compared to the bacterial activity (Baer et al.,
148 2015).

149 **2.2 Brine volume fraction and Raleigh number**

150 The brine volume fraction is used here as a proxy of sea ice permeability and is calculated from
151 the ice temperature and salinity following the relationship of Cox and Weeks (1983). We
152 assume that the sea ice was permeable for a brine volume fraction exceeding 5 % (Golden et
153 al., 1998). We also calculated the Rayleigh number (Ra), which is a proxy for brine convection
154 as described by Notz and Worster (2008). Theoretically, convection is possible in an ice layer
155 (of a thickness *h*) when Ra exceeds 1 and decreases from the top to the bottom of that layer
156 (Notz, personal communication). We thus simply assume the critical Ra being 1 following those
157 theoretical considerations.

158 **2.3 DOC and DON**

159 Samples for the determination of dissolved organic carbon (DOC) and total dissolved nitrogen
160 (TDN) were stored frozen (-20 °C) in glass vials (Wheaton; pre-combusted at 500 °C for 5 h)
161 and determined by high temperature catalytic oxidation and subsequent non-dispersive infrared
162 spectroscopy and chemiluminescence detection, respectively (TOC-VCPN, Shimadzu). After
163 each batch of five samples, one reference standard (DOC-DSR, Hansell Research Lab,
164 University of Miami, US), one ultrapure-water blank and one potassium hydrogen phthalate
165 standard for DOC and potassium nitrate for TDN were measured. DON concentrations were
166 calculated as difference of TDN and inorganic nitrogen. The accuracy of the measurements was
167 ± 5 %.

168 **2.4 Bacterial respiration**

169 Bacterial respiration has been calculated as the difference between the bacterial carbon demand
170 and bacterial production. We measured bacterial production (see below) and assumed that it
171 represented 34.8 % (bacterial growth efficiency, BGE) of the bacterial carbon demand to
172 deduce the bacterial respiration. BGE was derived as mean estimate from available sources for
173 sea-ice bacteria or bacteria in very cold temperatures (Kuparinen et al., 2011; Nguyen and
174 Maranger, 2011; Rivkin and Legendre, 2001).

175 For the bacterial production measurements, samples containing a known amount of crushed ice
176 and sterile-filtered seawater (Kaartokallio, 2004) were prepared in a cold room as follows: each
177 intact 5–10 cm ice core section was crushed using a spike and electrical ice cube crusher.
178 Approximately 10 mL of crushed ice was weighed in a scintillation vial. To better simulate the
179 brine pocket salinity and ensure an even distribution of labelled substrate, 3 ± 1 mL of sterile
180 filtered (through a 0.2 μm filter) seawater from the sample bags were added to the scintillation
181 vials. Bacterial production was measured immediately after sample collection using the [^{3}H]-
182 thymidine incorporation method (Fuhrman and Azam, 1982, 1980). Two aliquots and a
183 formaldehyde-fixed absorption blank were amended with [^{3}H]-thymidine (PerkinElmer, USA,
184 specific activity 20 Ci mmol^{-1}). The added concentration was 30 nmol L^{-1} for all sample types.
185 The samples were incubated in the dark at -0.6 °C on crushed ice in an insulated container
186 according to the projected level of activity: ice samples were incubated between 19 h and 22 h,
187 water and brine samples between 4 h and 6 h. The incubations were stopped by addition of
188 formaldehyde and samples were processed using the standard cold-TCA extraction and
189 filtration procedure. Samples were extracted for 15 minutes in ice-cold 5 % TCA and labelled
190 macromolecules collected on 0.2 μm mixed cellulose ester membrane filters (Osmonics). Filters

were rinsed five times with ice-cold 5% TCA and placed in clean scintillation vials. A Wallac WinSpectral 1414 counter and InstaGel (Perkin-Elmer) cocktail were used in scintillation counting. Bacterial production was calculated using a cell conversion factor of 2.09×10^{18} cells mol^{-1} (Smith and Clement, 1990), a cell volume of 0.3 μm^3 (Kaartokallio, 2004; Smith and Clement, 1990) and a carbon conversion factor of 0.12 pgC μm^{-3} (Nagata and Watanabe, 1990; Pelegrí et al., 1999).

2.5 pCO_2

The pCO_2 of the seawater was measured *in-situ* using a custom-made equilibration system, which is described in Delille et al. (2014). Briefly, the system consists of a membrane contractor equilibrator (Membrana®, Liqui-cell) that is connected to a non-dispersive infrared gas analyser (IRGA, Li-Cor® 6262) via a closed air loop. Seawater and air flow rates through the equilibrator and IRGA were approximately 2 L min^{-1} and 3 L min^{-1}, respectively. Temperature was simultaneously measured *in situ* and at the outlet of the equilibrator using Li-Cor® temperature sensors. Temperature correction of pCO_2 was applied assuming that the relation of Copin-Montegut (1988) is valid at low temperature and high salinity. Data were stored on a Li-Cor® Li-1400 data logger. All devices, except the peristaltic pump, were enclosed in an insulated box that contained a 12 V power source providing enough warming to keep the inside temperature above 0 °C. Uncertainty is less than 5 µatm.

The method for the pCO_2 measurements in ice is the same as in Geilfus et al. (2012b), but with longer equilibrium times following Crabeck et al. (2014). The ice samples were cut with a band saw, in a cold room at -25 °C and adjusted to the container's inner volume (4 cm x 4 cm x 4.4 cm). The sample was sanded down using fine-grained sandpaper so that it fitted tightly into the container to minimise the headspace volume. Then, the container was placed into a Dewar vessel filled with ethanol, which was cooled to -30 °C with liquid nitrogen. The container was then connected to the extraction line (tap closed). The line was first evacuated down to a pressure of 10^{-3} Torr, after which the container was evacuated for 5 min. The low temperature of the vessel insures sea ice impermeability, i.e., the CO_2 of the ice was not vacuumed during this process. The standard gas was then injected into the container at 1013 mbar. The container was subsequently removed from the extraction line (tap closed), placed in a thin plastic bag and submerged in a thermostatic bath (set to the *in situ* temperature, i.e., that was measured on the ice samples directly after the extraction). After 20 h of equilibrium, the container was placed in a Dewar filled with ethanol cooled at the *in situ* temperature and reconnected to the evacuated (10^{-3} Torr) extraction line. At the same time, a water trap consisting of a Dewar filled with an

ethanol bath at -65 °C was placed on the line just before the GC. The gas was finally injected into the GC. Immediately after the injection, the ice sample temperature was measured using a calibrated thermometer (Testo 720®). Reproducibility of the measurement is 2.9%.

2.6 TA and DIC

Total alkalinity (TA) was measured on melted bulk ice and seawater samples. Ice cores were cut at a 2 cm-depth resolution (about 50 g of ice for each section) and melted. Melted bulk ice and seawater samples were poisoned with a solution of supersaturated $HgCl_2$ and then stored in the dark, until analysis (one year after the sampling). TA was measured by open-cell titration with 0.11 M HCl and the endpoints were determined according to Gran (1952). Routine analyses of Certified Reference Materials (provided by A. G. Dickson, Scripps Institution of Oceanography) ensured that the uncertainty of the TA measurements was less than 4 μmol kg^{-1}.

Dissolved inorganic carbon (DIC) was calculated from TA and pCO_2 using CO2SYS (Lewis and Wallace, 1998), the CO_2 acidity constants of Mehrbach et al. (1973) refitted according to Dickson and Millero (1987) and other constants advocated by DOE (1994). We assumed that the CO_2 dissociation constants were applicable at sub-zero temperatures as suggested by Marion (2001) and Delille et al. (2007). To compare DIC in seawater and in melted bulk ice, we normalized the DIC values to a salinity of 7 (DIC_7), for consistency with previous studies. The salinity of 7 is also the mean salinity of the ice in this study. Uncertainty of DIC_7 deduced from the reproducibility of TA and pCO_2 has been evaluated to be 0.8 μmol kg^{-1} using Monte Carlo procedure (Anderson, 1976).

2.7 Differences between the SW and SWR series and statistical tests

The ice thickness was different between the SW and SWR mesocosms (up to 3 cm (15 %) of difference) at day 14 and day 15. This was due to an unavoidable temperature gradient in the experimental basin (Zhou et al., 2014). In spite of the gradient of temperature in the experimental basin, we do not think that it has affected the results. The SW and SWR mesocosms sampled the same day were adjacent mesocosms located on the same row (minimizing the differences in physical conditions). For day-to-day sampling, the SW/SWR pairs of mesocosms were randomly selected in space. In spite of that random selection, we still could see a trend in the physical parameters (Zhou et al., 2014), which means that the temperature gradient in the experimental basin did not significantly bias our results. However, to be rigorous, when the ice thicknesses were different for SW and SWR, we calculated the difference of the parameters (e.g., pCO_2) on normalized ice depth, and then multiplied the

normalized ice depth by the ice thickness of the SW series. In addition, two parameters were assumed to be similar (i.e., no significant difference between the SW and SWR series), when a minimum similarity score of 0.95 was achieved.

3. Results

3.1 Physical sea ice conditions

As described in Zhou et al. (2014), the differences in the physical properties of the ice between the SW and SWR mesocosms were insignificant. The brine volume fraction was above 5 % during the whole experiment, which suggests that the ice was always permeable (Golden et al., 1998). The maxima in the brine volume fraction were all found at the bottom of the ice, while the minima were found in the ice interior, and decreased from 13.3 % on day 1 to 5.7 % on day 14, but increased from day 15 onwards, due to the increase of the air temperature from -14 °C to -1 °C. The Rayleigh numbers were higher than 1, indicating favourable conditions for brine convection at all ice depths on day 2, and thereafter only at the bottom of the ice until day 14. From day 15 onwards, the Rayleigh numbers were always below 1, indicating that brine convection was unlikely (Figure 2). A large difference of Ra has been observed at the bottom of the ice between SW and SWR mesocosms, from day 6 to 14, and was likely due to an underestimation of salinity in SWR, and the propagation of that bias in the calculation of Ra (Zhou et al., 2014), but is not significant for the purpose of the present study.

3.2 DOC and DON

DOC concentrations in sea ice and water and their difference between the SW and the SWR mesocosms have been presented and discussed in Zhou et al. (2014) and Jørgensen et al. (2015). Most importantly, the salinity-normalized DOC concentrations in the underlying water were higher in the SWR mesocosms than in the SW mesocosm during the experiment (ppaired t-test, $p<0.001$); the medians were 142 µmol L^{-1} in SW and 246 µmol L^{-1} in SWR (salinity of 30.9), which were similar to the initial conditions. Median DOC concentrations in ice were 71 µmol L^{-1} in SW and 109 µmol L^{-1} in SWR. These are equivalent to 287 µmol L^{-1} and 409 µmol L^{-1} respectively, once normalized to a salinity of 30.9 as for the underlying water (paired t-test, $p<0.001$); they are higher than the values in water, which indicate a preferential retention of DOC in sea ice.

DON concentrations have not been systematically measured as for DOC (n=18 in water and 15 in ice for DON compared to n=20 and 110, respectively, for DOC (SW+SWR)). The limited

number of data we have show that the salinity-normalized DON concentrations were not significantly different in SW and SWR mesocosms, not before the experiment (median of 21 µmol L^{-1}), or during the experiment, in both the water and ice (medians of 17 µmol L^{-1} and 21 µmol L^{-1}, respectively) (data not shown). No significant trend in DON has been detected in the water and the ice over the experiment.

3.3 Bacterial activity

Median bacterial abundance in the underlying water increased over the experiment, reaching 1470 cells L^{-1} in SW and 1505 cells L^{-1} in SWR. This difference was not significant, despite the significantly higher bacterial production (BP) in the SWR mesocosms (paired t-test, p=0.007), with a median of 69 nmolC L^{-1} h^{-1} in SWR compared to 51 nmolC L^{-1} h^{-1} in SW. Bacterial respiration (BR) in water was also higher in the SWR mesocosms (paired t-test, p=0.027), with a median of 98 nmolC L^{-1} h^{-1} in SW and 129 nmolC L^{-1} h^{-1} in SWR, respectively (Figure 3a, left).

Median bacteria abundance in ice was 299 cells L^{-1} in SW and 352 cells L^{-1} in SWR, with a net loss of 24 cells $L^{-1}d^{-1}$ in SW and 16 cells $L^{-1}d^{-1}$ in SWR over the experiment. Median BP was 5 nmolC L^{-1} h^{-1} in SW and 13 nmolC L^{-1} h^{-1} in SWR, and median BR, 10 nmol L^{-1} h^{-1} in SW and 25 nmol L^{-1} h^{-1} in SWR (Fig. 3a, right). To compare bacterial activity in ice with that in seawater, we assumed that all these parameters were conservative against salinity. Once normalized to a salinity of 30.9, median bacterial abundance reached 1220 cells L^{-1} in SW and 1440 cells L^{-1} in SWR; median BP of 23 nmolC L^{-1} h^{-1} in SW and 53 nmolC L^{-1} h^{-1} in SWR; and median BR of 42 nmolC L^{-1} h^{-1} in SW and 100 nmolC L^{-1} h^{-1} in SWR. Note that all these values were higher in SWR than in SW (paired t-test, p<0.001), but lower than in seawater (paired t-test, p<0.001 for BP and BR in SWR; p=0.001 in SW; p=0.004 for bacterial abundance in SW but no significance has been found for bacterial abudnace in SWR). The vertical distribution of BR in ice was similar in the SW and SWR mesocosms (Figure 4): It increased from the top to the bottom of the ice. The difference between both mesocosm series generally increased from the top to the bottom of the ice, where the largest differences were observed.

3.4 DIC_7

For data comparison with litterature, we normalized DIC to a salinity of 7. Differences of DIC_7 between SW and SWR were not significant for both the under-ice water and the ice. DIC_7 in seawater varied around a median value of 455 µmol kg^{-1}, when excluding the outlier of SWR on day 5. Median DIC_7 in ice for the same mesocosms was slightly higher than in seawater,

reaching 486 µmol kg^{-1} (Figure 3). DIC_7 in both media increased from day 2 to day 16 and then remained constant. DIC_7 in the ice increased from the top to the bottom of the ice in SW and SWR mesocosms (Figure 5). At the bottom of the ice, it increased throughout the experiment and was always higher than the DIC_7 of the under-ice water by an average of 40 µmol kg^{-1}. The difference of DIC_7 between SWR and SW was higher in the ice interior at 8 cm to 12 cm depth. For comparison with bacterial respiration in ice, median DIC in ice that is not salinity-normalized was 434 µmol kg^{-1}, which is equivalent to 400 µmol L^{-1}.

3.5 pCO_2

pCO_2 in water was not significantly different between both mesocosm series, with a median pCO_2 of 270 ppm. pCO_2 in ice was also not significantly different between both mesocosm series probably as a result of the large variability. Median pCO_2 in ice was 360 ppm with a large range spanning from 223 ppm to 651 ppm (Figure 3). Median pCO_2 was higher in the ice than in seawater during ice growth (day 2 to day 14), despite similar concentrations of DIC_7 in the seawater and in the ice and lower bacterial respiration in ice than in seawater (Figure 3c, sections 3.3 and 3.4).

The pCO_2 in ice had a similar temporal evolution in the SW and SWR mesocosms (Figures 3c and 6). Considering that the average atmospheric pCO_2 was 460 ppm during the experiment (Kotovitch et al. submitted), pCO_2 in ice was at first under-saturated on day 2, and then became increasingly supersaturated until day 14, and then under-saturated again from day 15 onwards. Despite the similar temporal evolution of pCO_2 in ice, pCO_2 was generally higher in the SWR mesocosms, with a median value of 430 ppm compared to the 356 ppm in the SW mesocosms. The differences in pCO_2 were generally higher from the top to the ice interior to about 8 cm depth, except on day 2, when the ice was relatively thin (6 cm); on days 5 and 19, the difference of pCO_2 at the bottom of the ice was likely biased due to the large difference of CO_2 in the under-ice water (Figure 3c, left). Indeed, for days 5 and 19, the differences in pCO_2 in the under-ice water between SW and SWR were 100 ppm and 86 ppm, respectively, while they generally approached 0 ppm to 20 ppm in the other mesocosms on all other sampling days (Figure 3c, left).

4. Discussion

The addition of river water led to an enrichment of the overall DOC concentrations in the SWR water, compared to SW, by a factor of 1.8 (251 µmol L^{-1} / 140 µmol L^{-1}). The preferential retention of DOC in sea ice during ice formation (Giannelli et al., 2001; Müller et al., 2013;

Zhou et al., 2014) led to a salinity-normalized DOC concentration in ice that was higher than the under-ice water (409 μmol L^{-1} / 287 μmol L^{-1}), but the difference of DOC enrichment between SWR and SW dropped to 1.4. The mechanisms underlying the preferential retention of DOC in sea ice is not fully understood, but other measurements during our experiment suggested that sea ice formation increases the lability of DOM in ice (Jørgensen et al., 2015). We therefore speculate that the more labile forms of DOM were better retained in sea ice than the more refractory ones. Because SWR contained a larger fraction of less labile terrestrial humic acids due to the addition of river water (Jørgensen et al., 2015), the DOC enrichment in ice in SWR was lower than in SW. We show below that the segregation of DOC between water and ice, in addition to the difference in temperature and salinity, likely contributed to the difference of bacterial activity in water and ice.

4.1 Impact of riverine DOC addition on bacterial activity

Available under-ice or partially ice covered water respiration estimates for Western Arctic vary from 19 to 39 nmol C L^{-1} h^{-1} (Kirchman et al., 2009; Nguyen and Maranger, 2011; Nguyen et al., 2012), which is an order of magnitude lower than our respiration estimate for water (median of 98 nmol C L^{-1} h^{-1} in SW and 129 nmol C L^{-1} h^{-1}). However, our experimental system was based on North Sea water with a high DOC content and added inorganic nutrients, which are both likely to support higher bacterial production than the more oligotrophic Arctic waters.

Assuming that bacterial activity took place 24 hours a day, a consumption of 23.3 μmol C L^{-1} in SW and 31.5 μmol C L^{-1} in SWR is necessary to support the observed BP over the 19-day experiment. These represent 16 % and 13 % of the DOC pool, respectively. However, no significant changes have been detected in the DOC and DON concentrations in the under-ice water, or in the concentrations of inorganic nutrients (Zhou et al., 2014). A possible explanation is that bacteria used particulate organic matter (POM) as a carbon source for growth, despite the large pool of DOC. We did not measure POM concentrations in our experiment, but considering the absence of protists and active algae in seawater (in spite of the use of unfiltered seawater), we assumed that they died in the mesocosms, providing an additional source of carbon for bacterial growth. If this assumption is correct, BP would represent a smaller fraction of the DOC pool. The fraction was likely smaller than 3 % in SW and 9 % in SWR (the standard deviation of DOC concentrations among the mesocosms in the initial waters), because we would have detected significant changes otherwise.

Although BP only represented a small fraction of the DOC pool, the addition of riverine DOC was the most plausible factor causing the significantly higher BP in the SW water, since all the other parameters (bacterial abundance, DON, inorganic nutrients, temperature, and presumably POC) were not significantly different between the SW and SWR mesocosms.

Published sea-ice respiration values originate from batch culture incubations using sea ice bacteria and are either derived from total Arctic sea ice community respiration measurements made in water phase incubations (Nguyen and Maranger, 2011) or from experimental systems with Baltic sea ice bacteria (Kuparinen et al., 2011). The estimated mean bacterial respiration in western Arctic ice was 50 nmol C L^{-1} h^{-1} (Nguyen and Maranger, 2011) and in the Baltic Sea experiments approximately 80 nmol C L^{-1} h^{-1} (Kuparinen et al., 2011). Our respiration estimate for ice was lower but of the same order of magnitude, despite major differences in methodology and experimental setup.

Bacterial activity in ice was different from that in the under-ice water. Bacterial abundance in sea ice was lower than in seawater, even when normalized to the same salinity. This has been observed before in similar experiments (Eronen-Rasimus et al., 2014) and likely resulted from the low ice temperature and high brine salinity, which favour the selection of psychrotrophic and psychrophilic bacteria (Helmke and Weyland, 1995).

Although the overall BP and bacterial abundance were lower in the ice than in the under-ice water, the ratio between both the SW and SWR mesocosms were more pronounced in the ice. Bacterial production in SWR ice was 2.6 times higher than in SW, i.e., twice as high as the ratio (SWR/SW) observed in the water. Bacterial abundance was 20 % higher than the SW ice, while no significant difference was found in the under-ice water. The only plausible factor driving these SWR/SW differences in ice was the higher DOC concentration in the SWR ice. Ice microalgae and protists were indeed absent (verified by microscopy) and no significant difference has been found in the DON concentrations and the physical properties of the ice.

It is curious as to why the differences of BP between both series of mesocosms were larger in ice (SWR/SW ratio of 2.6) than in the water (ratio of 1.3), considering that the differences of DOC concentrations between both mesocosms series decreased (ratio of 1.4 in ice compared to 1.8 in water). This might be associated with the changes of the organic matter quality towards more labile (bioavailable) forms in the ice during sea ice formation (Jørgensen et al., 2015). In seawater, the addition of riverine DOC promoted higher BP in the SWR mesocosms. In sea ice, the absolute DOC concentrations in SWR are not only higher than in SW, their lability might also have increased compared to the SWR under-ice water; both might explain the larger

difference of BP in ice between the SW and SWR mesocosms compared to the under-ice water. DOC can directly contribute to bacterial growth as a carbon source; it may also support the formation of exopolymeric substances (EPS) in growing sea ice (Aslam et al., 2012) – a substance that is known to support microorganisms survival under the extreme conditions in sea ice (Krembs et al., 2011). Further, it might also have favoured the development of a bacterial community that is different from that in SW, as it has been observed by Eronen-Rasimus et al. (2014).

4.2 Similarities of DIC and pCO_2 in ice in the SW and SWR mesocosms

DIC_7, which ranged from 423 μmol kg^{-1} to 512 μmol kg^{-1} (in SW and SWR), was consistent with previous measurements on natural sea ice (Geilfus et al., 2014, 2012a; Rysgaard et al., 2007). pCO_2 measurements for natural sea ice are scarce (Crabeck et al., 2014; Geilfus et al., 2014) and have been mainly obtained from the spring-summer period. Therefore, they were generally under-saturated relative to the atmosphere (i.e., below 400 ppm) (Crabeck et al., 2014; Geilfus et al., 2014). The pCO_2 below 400 ppm in ice during the decay period of our experiment was thus consistent with data from natural sea ice in spring and summer. Because of the lack of pCO_2 measurements in natural ice during ice growth (and especially in autumn), we extended the comparison to the pCO_2 in brine. Considering that the median ice temperature approached -4.5 °C during ice growth in this experiment (Zhou et al., 2014), and that temperature would correspond to a pCO_2 of about 800 ppm in Arctic sea ice brine (Figure 1), our in situ measurements of up to 724 ppm are realistic.

Brine concentration and dilution and gas transport are likely to be the two main physical processes determining the similarities in the temporal and vertical pattern of pCO_2 between the SW and SWR mesocosms (Figure 7). When plotting pCO_2 in ice (SW and SWR) against the brine volume fraction, 10 mesocosms over 14 (represented by the circles on Figure 7) followed a decreasing trend ($r^2 = 0.836$, $p < 0.03$). These events include the very beginning of ice growth (day 2) and the ice growth and ice decay, except day 5, day 15 and two other outliers.

When cooling an ice sample, part of the water present in the brine inclusion will freeze, forming a thicker surrounding pure ice matrix, which results in a higher concentration of the dissolved constituents into smaller brine inclusions. Therefore, pCO_2 in sea ice became increasingly supersaturated, as the brine volume fraction decreased (from day 0 to day 14). In contrast, when warming an ice sample, the surrounding pure ice matrix is expected to melt, increasing the size of the brine inclusion and diluting the concentration of the dissolved constituents in the brines.

447 pCO_2 in sea ice thus became under-saturated as a result of the warming air temperature (from
448 day 15 onwards) (Figures 6 and 7).

449 A rapid and one-time decrease of pCO_2 in ice was observed on day 15. This was a particular
450 event, occurring the day after the rapid increase of the air temperature, when the sea ice surface
451 temperature sharply increased from -10 °C to -2 °C within 20 hours (Kotovitch et al.,
452 submitted). Different processes may explain this drastic decrease of pCO_2, e.g., rapid release
453 of gas bubbles (Zhou et al., 2013) and/or melt of CO_2-poor surface ice layers and seepage of
454 the meltwater (Geilfus et al., 2014), while the equilibrium of air-ice pCO_2 occurs at a much
455 slower rate. However, considering that day 15 was a particular event, it is unlikely that these
456 pCO_2 changes would be representative of those observed in natural conditions, so we will not
457 further discuss the different plausible processes. Another outlier corresponded to the surface
458 ice layer, where ice melt might have induced the low pCO_2 (153 ppm). We currently have no
459 explanation for the other outlier on day 5. Nevertheless, excluding these data, pCO_2 was
460 significantly correlated with the brine volume fraction, which indicates the major role of brine
461 concentration and dilution in regulating pCO_2 in ice.

462 To further demonstrate the importance of brine concentration and dilution for pCO_2 dynamics,
463 we compared our values with the theoretical pCO_2 considering only the changes in temperature
464 and brine salinity. The theoretical pCO_2 was calculated using the CO2SYS program (Lewis and
465 Wallace, 1998), the constants of Goyet and Poisson (1989), and the median temperature,
466 salinity, total alkalinity and DIC in the parent water as initial conditions. We then used the
467 median ice salinity (6.3) to calculate the brine volume fraction associated with each prescribed
468 temperature. The theoretical pCO_2 (red curve in Figure 7) reproduced the observations well
469 between 10 % and 20 % of brine volume fraction (i.e., for about half of the data set), but
470 overestimated the pCO_2 in ice (up to 320 ppm, i.e., 44 %) for brine volume fractions below 10
471 %. We attribute this overestimation to a significant escape of CO_2 from the ice to the
472 atmosphere during ice growth, which is not taken into account by the CO2SYS. Another
473 explanation could be that the constants used in CO2SYS might be incorrect for sea ice, since
474 they were developed for temperature and salinity ranges of seawater, which are less extreme
475 than those of sea ice. However, the error in the estimate of pCO_2 should approach 10 %
476 according to Brown et al. (2014), when using TA and DIC as input parameters and the constants
477 of Goyet and Poisson (1989). Hence, the error on the seawater-derived constant is not great
478 enough to explain the difference in pCO_2 between the CO2SYS estimate and the observations,

and therefore the escape of CO_2 from the ice to the atmosphere remains the most plausible explanation.

The DIC_7 profiles confirm that gas transport through sea ice affected pCO_2 in ice (Figure 5), in addition to brine concentration and dilution. If sea ice would be a closed system, and the air-ice and ice-water exchange absent, DIC would be conservative against salinity. Hence, the value of DIC_7 would be the same at all ice depths and in seawater. In our study, the ice was always permeable, with the brine volume fraction always above 5 % (Golden et al., 1998). Gas exchange through the ice was thus possible and resulted in the deviation of the DIC_7 in ice from the conservative behaviour. Values of DIC_7 in ice that decreased from the bottom to the top of the ice indicate an escape of CO_2 from the surface of the ice to the atmosphere (Figure 5) (Geilfus et al., 2013), and the observed decrease was also consistent with the air-ice fluxes we have measured during the growth phase of this experiment (Kotovitch et al., submitted). At the bottom of the ice, DIC_7, which approached the values in the under-ice water, indicate that ice-water exchange took place, which was possible through brine convection (high Rayleigh number, Figure 2). The DIC_7 at the bottom of the ice increased throughout the entire period of ice growth, following the increase in DIC_7 in the under-ice water as a result of the expulsion of DIC from the ice and bacterial respiration in the water during ice growth (Figure 3) (Moreau et al., submitted).

4.3 Differences of DIC and pCO_2 in ice between the SW and SWR mesocosms

DIC_7 and pCO_2 in ice were higher in SWR than in SW. However, these differences between SW and SWR were not significant, despite the significantly higher BR in SWR, which should result in a larger accumulation of DIC and CO_2 in SWR. Because the dynamics of DIC_7 and pCO_2 not only depend on bacterial activity, but also on physical processes (which were the same in both SW and SWR), the absence of significant differences might indicate that the physical processes have offset the bacterial impact on DIC_7 and pCO_2. For instance, if the differences of DIC_7 and pCO_2 were only due to bacterial activity, it is curious as to why the largest differences of DIC_7 and pCO_2 were observed in the ice interior (Figures 5 and 6), instead of at the bottom of the ice, where the difference in bacterial respiration was the largest. We interpret this as the result of gas exchange at the air-ice and ice-water interfaces, in addition to bacterial respiration. Since the difference of pCO_2 was smaller between the bottom of the ice and the water than between the surface of the ice and the atmosphere, we conclude that ice-water exchange might have been more efficient than air-ice exchange in decreasing the difference of pCO_2 between SWR and SW due to bacterial respiration. This is in agreement with the higher Rayleigh

512 numbers observed at all times at the bottom of the growing sea ice, that indicate enhanced
513 convection and therefore exchanges with the under-ice water.

514 Bacterial respiration in bulk ice (10 nmolC L^{-1} h^{-1} in SW and 25 nmolC L^{-1} h^{-1}) over 19 days
515 only represent 1 to 3% of the stock of DIC (400 µmolC L^{-1}). It is therefore curious as to how
516 such a low bacterial respiration may have caused a significant difference of pCO_2 in the ice
517 interior. An explanation could be the increase of the buffering effect of the carbonate system
518 with the decrease of temperature and the increase of salinity in brine (brine concentration). The
519 chemical buffer factor ($\beta = \Delta pCO_2/\Delta DIC$) describes the change in pCO_2 relative to the DIC
520 change induced by an input (i.e., respiration) or output of dissolved CO_2. It results from the
521 interplay of equilibrium dissociation reactions of the carbonate system and is a function of
522 several physico-chemical conditions (Delille et al., 2005; Frankignoulle, 1994). In a closed
523 system, β of brines increases significantly with decreasing temperature and the associated
524 increase of brine salinity (Figure 8). Providing that bacterial respiration could explain the
525 accumulation of DIC, an increase of DIC (even small) can result in a larger increase in pCO_2
526 in cold saline brine compared to warmer underlying seawater (Figure 8). Considering that the
527 difference of DIC_7 in the ice interior approached 15 µmol kg^{-1} (Figure 5) and that at ß
528 approached 4 at -4.5 °C (median temperature of the ice), an expected difference of pCO_2 due
529 to buffer factor changes should approach 60 ppm, which is relatively close to our observation
530 (Figure 6).

531 An alternate explanation is the underestimation of the bacterial respiration in bulk ice. We
532 calculated bacterial respiration based on thymidine incorporation and different conversion
533 factors. Our choice of BGE might have led to an underestimation of the estimate of bacterial
534 respiration, as discussed in the next section,.

535 **4.4 Modelling the impact of bacterial respiration on pCO_2 in ice**

536 In a closed system, bacterial respiration would induce an accumulation of DIC. In our semi-
537 enclosed system, DIC also changed due to physical processes (ice-air and ice-water exchanges).
538 The interplay of these various processes makes it difficult to use a simple calculation to prove
539 (i) whether the difference in bacterial respiration caused the observed difference of DIC and
540 pCO_2 in the ice interior, and (ii) whether ice-air and ice-water exchanges have offset the
541 difference of DIC and pCO_2 caused by respiration at the surface and the bottom of the ice,
542 respectively.

To tackle these issues, we used the one-dimensional thermodynamic sea ice model of Moreau et al. (2015) which includes ice-air gas exchanges and sea ice carbon dynamics. The model features ice growth and melt, ice-air and ice-water exchanges, as well as representations of full inorganic carbon and basic organic carbon dynamics within the ice. For the model simulations, all the parameters used are those described in Moreau et al. (2015), except for biological activity where primary production was shut down in the model runs. Bacterial respiration is prescribed with the median values of the bacterial respiration for SW and SWR, i.e., 10 nmol C L^{-1} h^{-1} in SW and 25 nmol C L^{-1} h^{-1} in SWR, which corresponded to the use of a bacterial growth efficiency (BGE) of 0.348. Based on the initial conditions of the experiment, we prescribed the initial seawater TA and DIC concentrations (2244 µmol kg^{-1} and 2039 µmol kg^{-1}, respectively) and the initial sea ice TA and DIC concentrations (847 µmol kg^{-1} and 748 µmol kg^{-1}). The model was run over 19 days (duration of the experiment), with a 1-hour time step.

Because the model has different temporal and spatial resolutions than the observations, we decided to only compare the temporal evolution of the median values in the ice (modelled versus measured variables). Overall, the model reproduced the ice thicknesses, median ice temperatures and salinities, as well as the standing stock of DIC and the median pCO_2 in ice in the same magnitude as those observed (Figure 9).

We first ran the model with the median values of the observed bacterial respiration for SW and SWR by using a BGE of 0.348 (Kuparinen et al., 2011). Given these bacterial respiration rates, the model reproduces the spatial pattern of the observed DIC_7 standing stock and the median pCO_2 (Figure 9) but not the magnitude of their difference between SW and SWR (Table 1). Therefore, we re-calculated bacterial respiration rates for SW and SWR using different BGE. Reducing BGE to 0.2 or 0.15 is plausible considering that BGE ranges from 0.05 to 0.6 (i.e., from 5 % to 60 %), depending on the environmental conditions (e.g., the quality of the dissolved organic matter) (Del Giorgio and Cole, 1998; Nguyen et al., 2012; Rivkin and Legendre, 2001).

Firstly, changing the BGE to 0.2 or 0.15, and hence increasing the BR, did not change the total stock of DIC and the median pCO_2 significantly (Figure 9, coloured curves), which supports our previous suggestions about the importance of the physical processes, such as brine concentration and dilution and gas transport, in regulating the dynamics of DIC and pCO_2 in sea ice. However, changing the BGE to 0.2 or 0.15 enhanced the differences in DIC_7 and pCO_2 in ice between SW and SWR (Table 1). The modelled median difference of DIC_7 fits the observations better when using a BGE of 0.2 and 0.15 (Table 1), and considering the reproducibility of +/- 0.8 µmol kg^{-1} for DIC. The median difference of pCO_2 is then higher than

576 the observed differences in pCO_2 between SW and SWR, but considering that the model slightly
577 overestimates the pCO_2 near the ice surface (*Kotovitch et al.*, submitted), differences in DIC_7,
578 rather than pCO_2, would be a better indicator of the difference in bacterial impact. The model
579 simulations therefore suggest that the bacterial respiration in ice might be up to 3 times higher
580 than our previous estimate (Table 1).

581 The estimate of BGE for the entire period of the experiment (0.15 - 0.2), as suggested by the
582 model simulations, was lower than assumed. Our BGE estimate of 0.348 was based on
583 empirical values obtained in liquid batch cultures in above-zero temperature (Kuparinen et al.
584 2011, Nguyen and Maranger 2011) combined with calculated temperature-dependent estimate
585 (Rivkin & Legendre 2001). Measuring bacterial process rates, especially respiration in sea-ice
586 systems is complicated and direct respiration measurements were not available. The lower
587 actual BGE suggested by the model in our experimental system compared to the previous
588 published values is plausible because of the extremely low temperatures and high salinities in
589 brine. Extreme conditions are in general forcing bacteria to invest more energy for survival than
590 for growth. Along these lines, the actual BGE may vary throughout the ice growth, being lower
591 during ice growth (where the conditions were more extreme), and higher during ice melt (where
592 the conditions were milder). Further investigations are encouraged to verify this hypothesis.
593 Furthermore, BGE in water column and ice may be different with higher BGE in water where
594 conditions are less extreme. Higher BGE from 0.4 to 0.5 were suggested by Moreau et al.
595 (submitted) for the under-ice water, in the same experimental system. Higher BGE for under-
596 ice water would also lower the respiration estimate towards values measured in other studies
597 (Kirchman et al. 2009, Nguyen and Maranger 2011, Nguyen et al. 2012) albeit in the high Arctic
598 under different nutrient and dissolved organic carbon regimes.

599 The comparison of Figure 5 with Figure 10, and Figure 6 with Figure 11 shows that the model
600 reproduced the temporal and spatial pattern of DIC_7 and pCO_2 well. DIC_7 decreased from the
601 bottom to the top of the ice due to air-ice gas exchange, except in the bottom most layer where
602 DIC_7 is underestimated due to an improper parameterization of heat and salt transfer in this
603 layer (Moreau et al., 2014; Vancoppenolle et al., 2010). pCO_2 was supersaturated in the ice
604 during the entire ice growth period, except in the bottom layer where brine convection pulled
605 the pCO_2 towards the under-saturated pCO_2 value of the under-ice water. pCO_2 in ice then also
606 became under-saturated, as it was observed, as a result of the increase of air temperature (and
607 the related brine dilution). In addition, due to the higher bacterial respiration in SWR compared
608 to SW, DIC_7 and pCO_2 were higher in SWR than in SW. The differences of pCO_2 are alleviated

609 at the bottom of the ice because of brine convection, and slightly at the top of the ice due to air-
610 ice gas exchange, but they are greater in the ice interior, which has to be associated with the
611 difference in bacterial respiration – the sole difference between the two runs: SW and SWR.

612 There are two main differences between the model simulations and the observations: The
613 absolute values of DIC_7 and pCO_2 are higher in the model than in the observations, and the
614 differences of DIC_7 and pCO_2 between SWR and SW present a smoother pattern in the model
615 than in the observations (Figures 5, 6, 9 and 10). Ice-air gas fluxes are currently not yet well
616 constrained in the model, resulting in a slight underestimation of the ice-air gas fluxes, and thus
617 an overestimation of the modeled DIC and pCO_2 content in the ice (Kotovitch et al., submitted).
618 The smoother pattern in the modelled differences of DIC_7 and pCO_2 may result from the higher
619 spatial and temporal resolution in the model than in the observations: Hourly time step and
620 calculation on the 10 ice layers in the model compared to the almost daily sampling with 1 to 4
621 measured ice layers on each ice core.

622 In brief, differences exist between the model simulations and the observations, probably due to
623 the parameterization of air-ice gas exchange and the difference of spatial and temporal
624 resolution, but the model was able to reproduce the temporal and spatial patterns of DIC_7 and
625 pCO_2, confirming therefore the importance of brine concentration and dilution, and gas
626 transport in controlling their dynamics. Most importantly, the model reproduced the observed
627 median difference of DIC_7 in the ice by introducing the measured bacterial respiration (for a
628 lower BGE of 0.15 or 0.2), confirming that higher bacterial respiration could indeed cause a
629 larger accumulation of DIC and a larger pCO_2 in the ice.

630 A corollary to the higher bacterial respiration, DIC and pCO_2 in SWR in the model is an
631 enhanced ice-air CO_2 flux during ice growth by 17 % (1.68 mmol m^{-2} d^{-1} and 1.97 mmol m^{-2} d^{-1}
632 in SW and SWR, respectively), and a reduced CO_2 flux during ice decay by 38 % (-1.52 mmol
633 m^{-2} d^{-1} and -0.93 mmol m^{-2} d^{-1} in SW and SWR, respectively) if we assume a BGE of 0.15
634 (simulated fluxes not shown). The enhanced CO_2 fluxes during ice growth are obviously due to
635 the higher pCO_2 in the ice resulting from the higher bacterial respiration. The negative CO_2
636 fluxes (i.e., from the air to the ice) are due to brine dilution (e.g., Nomura et al., 2010), and the
637 flux is less negative in SWR because the larger bacterial respiration in SWR better compensates
638 the effect of brine dilution. The integrated CO_2 flux over the 19 days of the simulation was 0.16
639 mmol m^{-2} d^{-1} and 1.04 mmol m^{-2} d^{-1} in SW and SWR, respectively. Hence, the addition of DOC
640 might have induced an air-ice CO_2 flux that was more than 6 times higher than without the
641 addition of DOC.

5. Conclusion and large scale implications

The aim of the study was to verify the hypothesis as to whether a larger input of riverine DOC in the Arctic water could induce a higher DOC concentration in sea ice, which would promote bacterial respiration, leading to a higher pCO_2 in brine. Although the overall trend of pCO_2 in both mesocosm series strongly depends on the ice temperature (Figure 1) as a result of the effect of brine concentration and brine dilution, the differences (SWR-SW) in observations and model simulations support our hypothesis.

The difference of pCO_2 between SW and SWR was much lower than the difference of pCO_2 in brine between the Arctic Ocean and the Southern Ocean. However, if we have added more labile DOC instead of humic-rich riverine water to our mesocosms and if we extended the duration of the experiment with lower air temperature, we may have observed larger differences of DIC and pCO_2, closer to those observed in natural conditions. The availability of more labile autochthonous DOC may promote higher bacterial respiration and higher accumulation of CO_2 in ice. Further, extending the duration of the experiment to several months, with further decrease of the ice temperature, would increase the respiration burden, reduce the ice permeability, and therefore reduce gases and DIC losses through the ice.

Because the addition of riverine DOC to seawater causes larger pCO_2 in ice, the Arctic Ocean, which receives a large input of terrestrial DOC through rivers, might induce more positive (or less negative) ice-air CO_2 fluxes than the Southern Ocean, for the same environmental conditions. Similarly, Arctic coastal waters might also be associated with a more positive (or negative) ice-air CO_2 fluxes than the central Arctic. This is at least true for the ice growth period when algal growth is limited, as considered by the absence of autochthonous DOC in our experiment. Algal growth would consume CO_2 but will also produce labile autochtonous DOC that enhances bacterial production. Further experiments are therefore needed to refine the net impact of algal and bacterial growth on pCO_2 in ice and on the inter-hemispheric differences.

The inter-hemispheric difference of pCO_2 in ice and brine likely results from the impact of ice temperature on the ice permeability and the buffering effect of the carbonate system, in addition to the DOC input. Lower ice temperatures are associated with larger buffering effects, i.e., the increase of pCO_2 in the ice interior in response to a given increase of DIC (due to bacterial respiration) would be enhanced. If the ice temperature is low enough so that the ice becomes impermeable to gas exchange, the accumulation of pCO_2 would have been more obvious, resulting in the larger observed inter-hemispheric difference of pCO_2 in ice and brine. On the contrary, higher ice temperatures are associated with lower buffering effects and larger ice

permeability. Exchange may occur through the ice, and offset the bacterial accumulation of CO_2. In our study, the impact of bacterial respiration on pCO_2 was most obvious in the ice interior, because ice-air gas exchange and brine convection have offset the increase of pCO_2 associated with bacterial respiration at the ice interfaces.

Considering the drastic decline in Arctic sea ice, we may also wonder how air-sea and air-ice CO_2 fluxes may change in the future. If the ice cover is replaced more and more by open water, the most common scenario is that air-sea CO_2 fluxes increase, because gas exchange is more efficient via an open sea surface than a semi-permeable ice cover. Our work highlighted the fact that the dynamics regulating the pCO_2 gradient will be different too. Due to the buffering effect of the carbonate system, brine concentration makes the pCO_2 more sensitive to DIC increase in ice than in seawater, and a small accumulation of DIC, due to low bacterial respiration may result in a large increase of pCO_2 in the ice. At some specific locations, where bacterial activity is more intense in the ice than in the underlying water, the consequence of bacterial respiration on pCO_2 in ice may be even more significant, especially when algal activity is limited. The interplay between gas transfer velocity and the pCO_2 gradient needs to be taken into consideration while assessing the future evolution of the air-sea and air-ice CO_2 fluxes in the polar regions.

Acknowledgments

We are grateful to two anonymous reviewers for their useful comments which have improved the quality of the manuscript. This study was supported by the European Community's 7th Framework Programme through the grant to the budget of the Integrated Infrastructure Initiative HYDRALAB-IV, Contract no. 261520. The authors would like to thank the Hamburg Ship Model Basin (HSVA), Karl-Ulrich Evers and the rest of the ice tank crew, for the hospitality, technical and scientific support and the professional execution of the test program in the Research Infrastructure ARCTICLAB. The work was supported by a FiDiPro award by the Academy of Finland, the Walter and Andree Nottbeck Foundation, and the BIGSOUTH project funded by the Belgian Science Federal Policy Office. MK, SM and BD are respectively research fellows, postdoctoral researcher and research associate of the Fonds de la Recherche Scientique –FNRS. JZ was a F.R.S.-FNRS research fellow and is presently a BAEF Francqui Foundation research fellow. This is a MARE contribution n°XXX.

Contributions

JLT, BD, GD, HK, GK planned and designed the experiment under the lead of DT; JZ, MK, JLT, BD, GD and DT provided the data on sea ice physics and carbonate chemistry, HK, the bacterial data, GK, the DOC data, and SM, the model simulations. JZ, BD, HK, SM wrote the paper with the valuable comments and inputs from all the other co-authors.

Captions

Figure 1. pCO_2 measurements in sea ice and brine in the Arctic and Antarctica after Geilfus et al. (2014), excluding the measurements where flooding was observed. The horizontal line indicates a pCO_2 of 400ppm - a reference value considering current atmospheric pCO_2.

Figure 2. Brine volume fraction (BrV, in %) and Rayleigh number (Ra) in the SW and SWR mesocosms during the experiment. The black dots are the data points from the sampling, while the color in between results is from interpolation (natural neighbours in Surfer 8 © software) (Zhou et al., 2014).

Figure 3. a) Bacterial respiration (BR_TdR), b) DIC_7 and c) pCO_2 in water and sea ice. Note that for sea ice, we plotted the median value of each ice core.

Figure 4. Bacterial respiration (BR_TdR) in ice in the SW and SWR mesocosms during the experiment, and the difference between both mesocosms. Bacterial respiration is expressed in nmol C L^{-1} h^{-1}.

Figure 5. DIC_7 in ice of the SW and SWR mesocosms during the experiment, and the difference between both mesocosms. DIC_7 is expressed in µmol C kg^{-1}. Insignificant differences of DIC_7 are set in white.

Figure 6. pCO_2 in ice in the SW and SWR mesocosms during the experiment, and the difference between both mesocosms. pCO_2 is expressed in ppm. Insignificant differences of pCO_2 are set in white.

Figure 7. Relationship between pCO_2 in ice and brine volume fraction. The circles are the data used to draw the fit (black curve), the other discrete symbols are not considered (see explanation in the text). The blue curves are the 95 % confidence bands of the fit and the red dashed curve is the relationship predicted by CO2SYS (Lewis and Wallace, 1998).

Figure 8. Buffer factor of the carbonate system for decreasing temperature and related increase of salinity due to brine concentration/dilution in a closed system. Initial conditions was S = 35.17, T = -1.8 °C, TA = 2578 µmol kg^{-1}, DIC = 2450.4 µmol kg^{-1}, pCO_2 = 400 µatm. β is provided for an increase of DIC of 20 µmol kg^{-1}.

Figure 9. (Clockwise) Temporal changes of the ice thickness, median ice temperature, median ice salinity, the standing stock of DIC and the median pCO_2 in the ice. The dots refer to the measurements (white for SW and black for SWR), while the curves refer to the simulated results. The vertical dashed line shows the transition from ice growth to ice decay.

Figure 10 Modeled DIC_7 in ice, in SW and SWR mesocosms, and the difference SWR minus SW, using a median bacterial respiration in ice associated with a BGE of 0.15 (Table 1).

Figure 11. Modeled pCO_2 in ice, in SW and SWR mesocosms, and the difference SWR minus SW, using a median bacterial respiration in ice associated with a BGE of 0.15 (Table 1).

Table 1. Calculated median bacterial respiration (BR) in ice in SW and SWR using different bacterial growth efficiencies (BGE), the measured median difference of pCO_2 and DIC (SWR minus SW) during the experiment (Diff pCO_2 and Diff DIC_7), and the modeled difference of pCO_2 and DIC for each set of BGE-dependent BR.

References

Anderson, G.M., 1976. Error propagation by the Monte Carlo method in geochemical calculations. Geochim. Cosmochim. Acta 40, 1533–1538.

Aslam, S.N., Underwood, G.J.C., Kaartokallio, H., Norman, L., Autio, R., Fischer, M., Kuosa, H., Dieckmann, G.S., Thomas, D.N., 2012. Dissolved extracellular polymeric substances (dEPS) dynamics and bacterial growth during sea ice formation in an ice tank study. Polar Biol. 35, 661–676. doi:10.1007/s00300-011-1112-0

Baer, S., Connelly, T., Bronk, D., 2015. Nitrogen uptake dynamics in landfast sea ice of the Chukchi Sea. Polar Biol. 38, 781–797. doi:10.1007/s00300-014-1639-y

Brown, K.A., Miller, L.A., Davelaar, M., Francois, R., Tortell, P.D., 2014. Over-determination of the carbonate system in natural sea-ice brine and assessment of carbonic acid dissociation constants under low temperature, high salinity conditions. Mar. Chem. 165, 36–45. doi:10.1016/j.marchem.2014.07.005

Copin-Montegut, C., 1988. A new formula for the effect of temperature on the partial pressure of CO2 in seawater. Mar. Chem. 25, 29–37. doi:10.1016/0304-4203(88)90012-6

Cox, G.F.N., Weeks, W.F., 1983. Equations for determining the gas and brine volumes in sea ice samples. J. Glaciol. 29, 306–316.

Crabeck, O., Delille, B., Thomas, D., Geilfus, N.-X., Rysgaard, S., Tison, J.-L., 2014. CO2 and CH4 in sea ice from a subarctic fjord under influence of riverine input. Biogeosciences 11, 6525–6538. doi:10.5194/bg-11-6525-2014

Del Giorgio, P., Cole, J.J., 1998. Bacterial growth efficiency in natural aquatic systems. Annu. Rev. Ecol. Syst. 29, 503–541.

Delille, B., 2006. Inorganic carbon dynamics and air-ice-sea CO2 fluxes in the open and coastal waters of the Southern Ocean. Université de Liège, Belgique.

Delille, B., Harlay, J., Zondervan, I., Jacquet, S., Chou, L., Wollast, R., Bellerby, R.G.J., Frankignoulle, M., Borges, A.V., Riebesell, U., Gattuso, J.P., 2005. Response of primary production and calcification to changes of pCO2 during experimental blooms of the coccolithophorid Emiliania huxleyi. Global Biogeochem. Cycles 19, 1–14. doi:10.1029/2004GB002318

Delille, B., Jourdain, B., Borges, A. V., Tison, J.-L., Delille, D., 2007. Biogas (CO2, O2, dimethylsulfide) dynamics in spring Antarctic fast ice. Limnol. Oceanogr. 52, 1367–1379. doi:10.4319/lo.2007.52.4.1367

Delille, B., Vancoppenolle, M., Geilfus, N.-X., Tilbrook, B., Lannuzel, D., Schoemann, V., Becquevort, S., Carnat, G., Delille, D., Lancelot, C., Chou, L., Dieckmann, G.S., Tison, J.-L., 2014. Southern Ocean CO2 sink: The contribution of the sea ice. J. Geophys. Res. Ocean. 119, 6340–6355. doi:10.1002/2014JC009941

789 Dickson, A.G., Millero, F.J., 1987. A comparison of the equilibrium constants for the
790 dissociation of carbonic acid in seawater media. Deep Sea Res. 34, 1733–1743.
791 doi:10.1016/0198-0149(87)90021-5

792 Dieckmann, G.S., Nehrke, G., Papadimitriou, S., Göttlicher, J., Steininger, R., Kennedy, H.,
793 Wolf-Gladrow, D., Thomas, D.N., 2008. Calcium carbonate as ikaite crystals in
794 Antarctic sea ice. Geophys. Res. Lett. 35, 35–37. doi:10.1029/2008GL033540

795 Dieckmann, G.S., Nehrke, G., Uhlig, C., Göttlicher, J., Gerland, S., Granskog, M.A., Thomas,
796 D.N., 2010. Brief Communication: Ikaite (CaCO3·6H2O) discovered in Arctic sea ice.
797 Cryosphere 4, 227–230. doi:10.5194/tc-4-227-2010

798 Dittmar, T., Kattner, G., 2003. The biogeochemistry of the river and shelf ecosystem of the
799 Arctic Ocean: a review. Mar. Chem. 83, 103–120. doi:10.1016/S0304-4203(03)00105-1

800 DOE, 1994. Handbook of Methods for the Analysis of the Various Parameters of the Carbon
801 Dioxide System in Sea Water; version2.

802 Eronen-Rasimus, E., Kaartokallio, H., Lyra, C., Autio, R., Kuosa, H., Dieckmann, G.S.,
803 Thomas, D.N., 2014. Bacterial community dynamics and activity in relation to dissolved
804 organic matter availability during sea-ice formation in a mesocosm experiment.
805 Microbiologyopen 3, 139–156. doi:10.1002/mbo3.157

806 Frankignoulle, M., 1994. A complete set of buffer factors for acid/base CO2 system in
807 seawater. J. Mar. Syst. 5, 111–118. doi:10.1016/0924-7963(94)90026-4

808 Fuhrman, J.A., Azam, F., 1982. Thymidine incorporation as a measure of heterotrophic
809 bacterioplankton production in marine surface waters: Evaluation and field results. Mar.
810 Biol. 66, 109–120. doi:10.1007/BF00397184

811 Fuhrman, J.A., Azam, F., 1980. Bacterioplankton secondary production estimates for coastal
812 waters of British Columbia, Antarctica, and California. Appl. Environ. Microbiol. 39,
813 1085–1095.

814 Geilfus, N.-X., Carnat, G., Dieckmann, G.S., Halden, N., Nehrke, G., Papakyriakou, T.,
815 Tison, J.-L., Delille, B., 2013. First estimates of the contribution of CaCO3 precipitation
816 to the release of CO2 to the atmosphere during young sea ice growth. J. Geophys. Res.
817 Ocean. 118, 244–255. doi:10.1029/2012JC007980

818 Geilfus, N.-X., Carnat, G., Papakyriakou, T., Tison, J.-L., Else, B., Thomas, H., Shadwick, E.,
819 Delille, B., 2012a. Dynamics of pCO2 and related air-ice CO2 fluxes in the Arctic
820 coastal zone (Amundsen Gulf, Beaufort Sea). J. Geophys. Res. Ocean. 117, C00G10.
821 doi:10.1029/2011JC007118

822 Geilfus, N.-X., Delille, B., Verbeke, V., Tison, J.-L., 2012b. Towards a method for high
823 vertical resolution measurements of the partial pressure of CO2 within bulk sea ice. J.
824 Glaciol. 58, 287–300. doi:10.3189/2012JoG11J071

825 Geilfus, N.-X., Tison, J.-L., Ackley, S.F., Galley, R.J., Rysgaard, S., Miller, L.A., Delille, B.,
826 2014. Sea ice pCO2 dynamics and air-ice CO2 fluxes during the Sea Ice Mass Balance in

827 the Antarctic (SIMBA) experiment – Bellingshausen Sea, Antarctica. Cryosph. 8, 2395–
828 2407. doi:10.5194/tc-8-2395-2014

829 Giannelli, V., Thomas, D.N., Haas, C., Kattner, G., Kennedy, H., Dieckmann, G.S., 2001.
830 Behaviour of dissolved organic matter and inorganic nutrients during experimental sea-
831 ice formation. Ann. Glaciol. 33, 317–321. doi:10.3189/172756401781818572

832 Golden, K.M., Ackley, S.F., Lytle, V.I., 1998. The percolation phase transition in sea ice.
833 Science (80-.). 282, 2238–2241. doi:10.1126/science.282.5397.2238

834 Gosink, T.A., Pearson, J.G., Kelley, J.J., 1976. Gas movement through sea ice. Nature 263,
835 41–42.

836 Goyet, C., Poisson, A., 1989. New determination of carbonic acid dissociation constants in
837 seawater as a function of temperature and salinity. Deep Sea Res. 36, 1635–1654.
838 doi:10.1016/0198-0149(89)90064-2

839 Gran, G., 1952. Determination of the Equivalence Point in Potentiometric Titrations. Part II.
840 Analyst 77, 661–671.

841 Hansell, D., Carlson, C., Repeta, D., Schlitzer, R., 2009. Dissolved Organic Matter in the
842 Ocean: A Controversy Stimulates New Insights. Oceanography.
843 doi:10.5670/oceanog.2009.109

844 Helmke, E., Weyland, H., 1995. Bacteria in sea ice and underlying water of the eastern
845 Weddell Sea in midwinter. Mar. Ecol. Prog. Ser. 117, 269–288.
846 doi:10.3354/meps117269

847 Hunke, E.C., Notz, D., Turner, A.K., Vancoppenolle, M., 2011. The multiphase physics of sea
848 ice: a review for model developers. Cryosph. 5, 989–1009. doi:10.5194/tc-5-989-2011

849 Jørgensen, L., Stedmon, C. a., Kaartokallio, H., Middelboe, M., Thomas, D.N., 2015.
850 Changes in the composition and bioavailability of dissolved organic matter during sea
851 ice formation. Limnol. Oceanogr. 00, 00–00. doi:10.1002/lno.10058

852 Kaartokallio, H., 2004. Food web components, and physical and chemical properties of Baltic
853 Sea ice. Mar. Ecol. Prog. Ser. 273, 49–63. doi:10.3354/meps273049

854 Kirchman, D.L., Hill, V., Cottrell, M.T., Gradinger, R., Malmstrom, R.R., Parker, A., 2009.
855 Standing stocks, production, and respiration of phytoplankton and heterotrophic bacteria
856 in the western Arctic Ocean. Deep. Res. Part II Top. Stud. Oceanogr. 56, 1237–1248.
857 doi:10.1016/j.dsr2.2008.10.018

858 Kotovitch, M., Moreau, S., Zhou, J., Goosse, H., Vancoppenolle, M., Dieckmann, G.S.,
859 Thomas, D.N., Tison, J.-L., Delille, B., n.d. Measurements of air-ice CO2 fluxes over
860 experimental sea ice emphasize the role of bubbles in gas transport during ice growth,
861 Elementa: Science of the Anthropocene.

862 Krembs, C., Eicken, H., Deming, J.W., 2011. Exopolymer alteration of physical properties of
863 sea ice and implications for ice habitability and biogeochemistry in a warmer Arctic.
864 Proc. Natl. Acad. Sci. U. S. A. 108, 3653–8. doi:10.1073/pnas.1100701108

865 Kuparinen, J., Autio, R., Kaartokallio, H., 2011. Sea ice bacterial growth rate, growth
866 efficiency and preference for inorganic nitrogen sources in the Baltic Sea. Polar Biol. 34,
867 1361–1373. doi:10.1007/s00300-011-0989-y

868 Lewis, E., Wallace, D.W.R., 1998. Program developed for CO2 system calculations.

869 Loose, B., McGillis, W.R., Perovich, D., Zappa, C.J., Schlosser, P., 2014. A parameter model
870 of gas exchange for the seasonal sea ice zone. Ocean Sci. 10, 17–28. doi:10.5194/os-10-
871 17-2014

872 Loose, B., Schlosser, P., Perovich, D., Ringelberg, D., Ho, D.T., Takahashi, T., Richter-
873 Menge, J., Reynolds, C.M., Mcgillis, W.R., Tison, J.-L., 2011. Gas diffusion through
874 columnar laboratory sea ice: implications for mixed-layer ventilation of CO2 in the
875 seasonal ice zone. Tellus B 63, 23–39. doi:10.1111/j.1600-0889.2010.00506.x

876 Marion, G.M., 2001. Carbonate mineral solubility at low temperatures in the Na-K-Mg-Ca-H-
877 Cl-SO4-OH-HCO3-CO3-CO2-H2O system. Geochim. Cosmochim. Acta 65, 1883–
878 1896.

879 Mehrbach, C., Culbrtdon, C.H., Hawley, J.E., Pytkowicz, R.M., 1973. Measurement of the
880 apparent dissociation constants of carbonic acid in seawater at atmospheric pressure.
881 Limnol. Oceanogr. 18, 897–907. doi:10.4319/lo.1973.18.6.0897

882 Miller, L.A., Carnat, G., Else, B.G.T., Sutherland, N., Papakyriakou, T.N., 2011a. Carbonate
883 system evolution at the Arctic Ocean surface during autumn freeze-up. J. Geophys. Res.
884 116, C00G04. doi:10.1029/2011JC007143

885 Miller, L.A., Papakyriakou, T.N., Collins, R.E., Deming, J.W., Ehn, J.K., Macdonald, R.W.,
886 Mucci, A., Owens, O., Raudsepp, M., Sutherland, N., 2011b. Carbon dynamics in sea
887 ice: A winter flux time series. J. Geophys. Res. 116, C02028.
888 doi:10.1029/2009JC006058

889 Moreau, S., Kaartokallio, H., Vancoppenolle, M., Zhou, J., Kotovitch, M., Dieckmann, G.S.,
890 Thomas, D.N., Goosse, H., Tison, J.-L., Delille, B., n.d. Closing the O2 and CO2 budget
891 under a growing ice sheet - a laboratory investigation, Elementa: Science of the
892 Anthropocene.

893 Moreau, S., Vancoppenolle, M., Delille, B., Tison, J.-L., Zhou, J., Kotovitch, M., Thomas,
894 D.N., Geilfus, N.-X., Goosse, H., 2015. Drivers of inorganic carbon dynamics in first-
895 year sea ice: A model study. J. Geophys. Res. Ocean. 120, 471–495.
896 doi:10.1002/2014JC010388

897 Moreau, S., Vancoppenolle, M., Zhou, J., Tison, J.-L., Delille, B., Goosse, H., 2014.
898 Modelling argon dynamics in first-year sea ice. Ocean Model. 73, 1–18.
899 doi:10.1016/j.ocemod.2013.10.004

900 Müller, S., Vähätalo, A. V., Stedmon, C. a., Granskog, M. a., Norman, L., Aslam, S.N.,
901 Underwood, G.J.C., Dieckmann, G.S., Thomas, D.N., 2013. Selective incorporation of
902 dissolved organic matter (DOM) during sea ice formation. Mar. Chem. 155, 148–157.
903 doi:10.1016/j.marchem.2013.06.008

904 Nagata, T., Watanabe, Y., 1990. Carbon- and nitrogen-to-volume ratios of bacterioplankton
905 grown under different nutritional conditions. Appl. Environ. Microbiol. 56, 1303–1309.

906 Nguyen, D., Maranger, R., 2011. Respiration and bacterial carbon dynamics in Arctic sea ice.
907 Polar Biol. 34, 1843–1855. doi:10.1007/s00300-011-1040-z

908 Nguyen, D., Maranger, R., Tremblay, J.É., Gosselin, M., 2012. Respiration and bacterial
909 carbon dynamics in the Amundsen Gulf, western Canadian Arctic. J. Geophys. Res.
910 Ocean. 117, 1–12. doi:10.1029/2011JC007343

911 Nomura, D., Eicken, H., Gradinger, R., Shirasawa, K., 2010. Rapid physically driven
912 inversion of the air–sea ice CO2 flux in the seasonal landfast ice off Barrow, Alaska after
913 onset of surface melt. Cont. Shelf Res. 30, 1998–2004. doi:10.1016/j.csr.2010.09.014

914 Notz, D., Worster, M.G., 2009. Desalination processes of sea ice revisited. J. Geophys. Res.
915 114, C05006. doi:10.1029/2008JC004885

916 Notz, D., Worster, M.G., 2008. In situ measurements of the evolution of young sea ice. J.
917 Geophys. Res. Ocean. 113, C03001. doi:10.1029/2007JC004333

918 Papadimitriou, S., Thomas, D.N., Kennedy, H., Haas, C., Kuosa, H., Krell, A., Dieckmann,
919 G.S., 2007. Biogeochemical composition of natural sea ice brines from the Weddell Sea
920 during early austral summer. Limnol. Oceanogr. 52, 1809–1823.
921 doi:10.4319/lo.2007.52.5.1809

922 Pelegrí, S.P., Dolan, J., Rassoulzadegan, F., 1999. Use of high temperature catalytic oxidation
923 (HTCO) to measure carbon content of microorganisms. Aquat. Microb. Ecol. 16, 273–
924 280. doi:10.3354/ame016273

925 Rivkin, R.B., Legendre, L., 2001. Biogenic carbon cycling in the upper ocean: effects of
926 microbial respiration. Science (80-.). 291, 2398–2400.

927 Rysgaard, S., Glud, R.N., Sejr, M.K., Bendtsen, J., Christensen, P.B., 2007. Inorganic carbon
928 transport during sea ice growth and decay: A carbon pump in polar seas. J. Geophys.
929 Res. 112, C03016. doi:10.1029/2006JC003572

930 Shadwick, E.H., Thomas, H., Chierici, M., Else, B., Fransson, A., Michel, C., Miller, L.A.,
931 Mucci, A., Niemi, A., Papakyriakou, T.N., Tremblay, J.-É., 2011. Seasonal variability of
932 the inorganic carbon system in the Amundsen Gulf region of the southeastern Beaufort
933 Sea. Limnol. Oceanogr. 56, 303–322. doi:10.4319/lo.2011.56.1.0303

934 Smith, R.E.H., Clement, P., 1990. Heterotrophic activity and bacterial productivity in
935 assemblages of microbes from sea ice in the high Arctic. Polar Biol. 10, 351–357.
936 doi:10.1007/BF00237822

937 Vancoppenolle, M., Goosse, H., de Montety, A., Fichefet, T., Tremblay, B., Tison, J.-L.,
938 2010. Modeling brine and nutrient dynamics in Antarctic sea ice: The case of dissolved
939 silica. J. Geophys. Res. 115, C02005. doi:10.1029/2009JC005369

940 Zhou, J., Delille, B., Eicken, H., Vancoppenolle, M., Brabant, F., Carnat, G., Geilfus, N.-X.,
941 Papakyriakou, T., Heinesch, B., Tison, J.-L., 2013. Physical and biogeochemical
942 properties in landfast sea ice (Barrow, Alaska): Insights on brine and gas dynamics
943 across seasons. J. Geophys. Res. Ocean. 118, 3172–3189. doi:10.1002/jgrc.20232

944 Zhou, J., Delille, B., Kaartokallio, H., Kattner, G., Kuosa, H., Tison, J.-L., Autio, R.,
945 Dieckmann, G.S., Evers, K.-U., Jørgensen, L., Kennedy, H., Kotovitch, M., Luhtanen,
946 A.-M., Stedmon, C.A., Thomas, D.N., 2014. Physical and bacterial controls on inorganic
947 nutrients and dissolved organic carbon during a sea ice growth and decay experiment.
948 Mar. Chem. 166, 59–69. doi:10.1016/j.marchem.2014.09.013

949

950

951
952

	Observations				Model	
	BR (SW)	**BR (SWR)**	**Diff pCO_2**	**Diff DIC_7**	**Diff pCO_2**	**Diff DIC_7**
	nmol C L^{-1} h^{-1}	nmol C L^{-1} h^{-1}	ppm	μmol kg^{-1}	ppm	μmol kg^{-1}
BGE = 0.348	10.0	24.7	13	2.8	8.3	0.9
BGE = 0.2	21.5	52.6			19.3	1.9
BGE = 0.15	30.4	74.6			31.9	2.7

Fig. 1

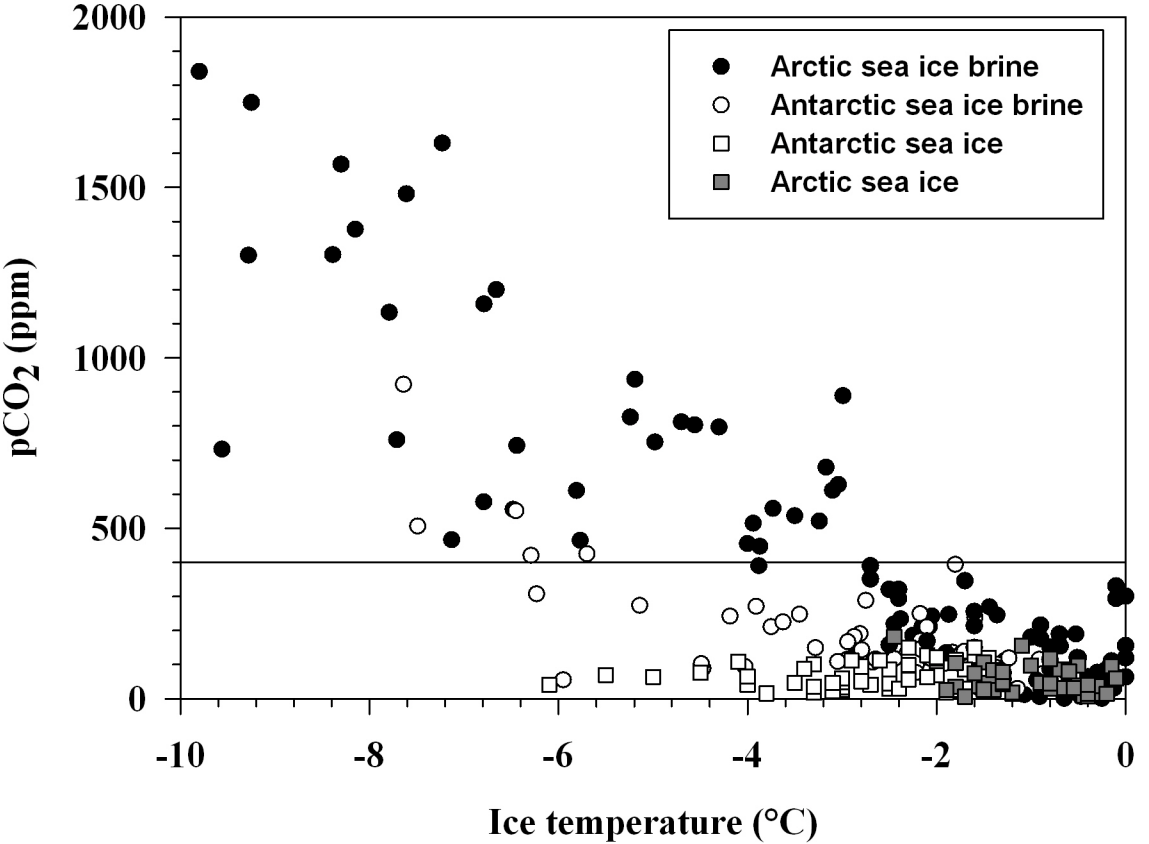
2000
1500
1000
500
0
pCO2 (ppm)
-10
-8
-6
-4
-2
0
Ice temperature (°C)
Arctic sea ice brine
Antarctic sea ice brine
Antarctic sea ice
Arctic sea ice

Fig. 2

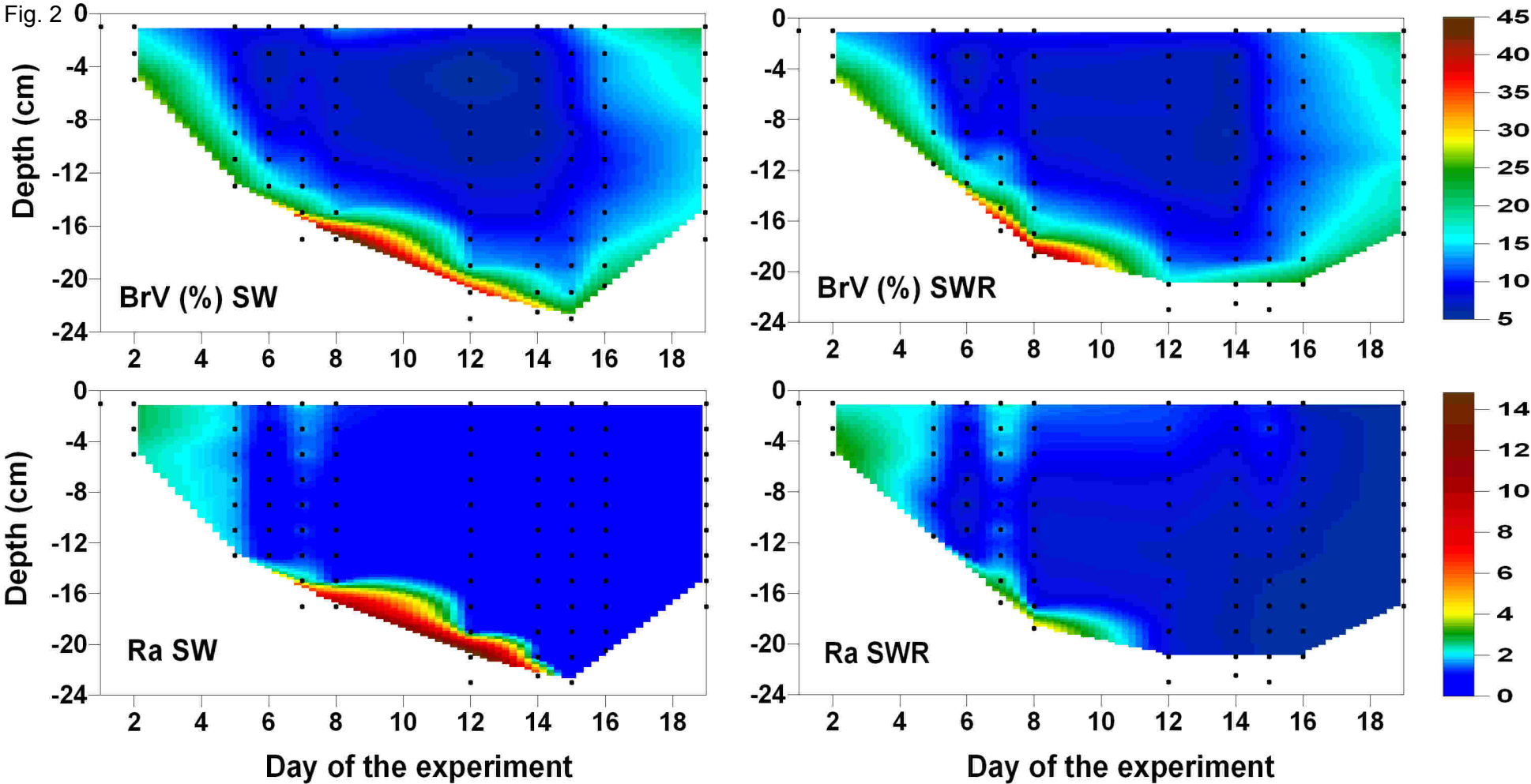
Depth (cm)
0
-4
-8
-12
-16
-20
-24
BrV (%) SW
BrV (%) SWR
Ra SW
Ra SWR
2
4
6
8
10
12
14
16
18
Day of the experiment
45
40
35
30
25
20
15
10
5
14
12
10
8
6
4
2
0

Fig.3

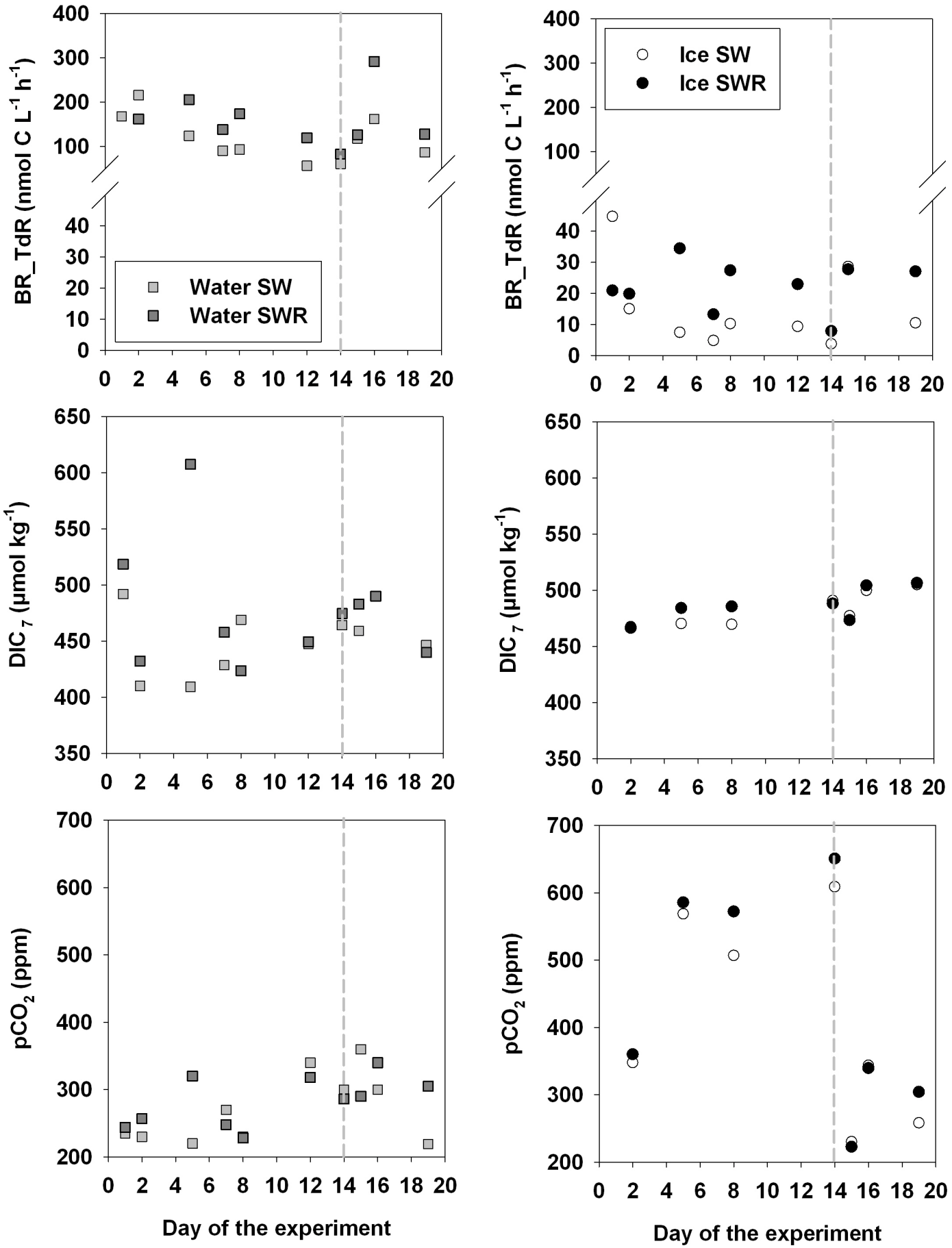
BR_TdR (nmol C L-1 h-1)
Water SW
Water SWR
Ice SW
Ice SWR
DIC7 (µmol kg-1)
pCO2 (ppm)
Day of the experiment

Fig. 4

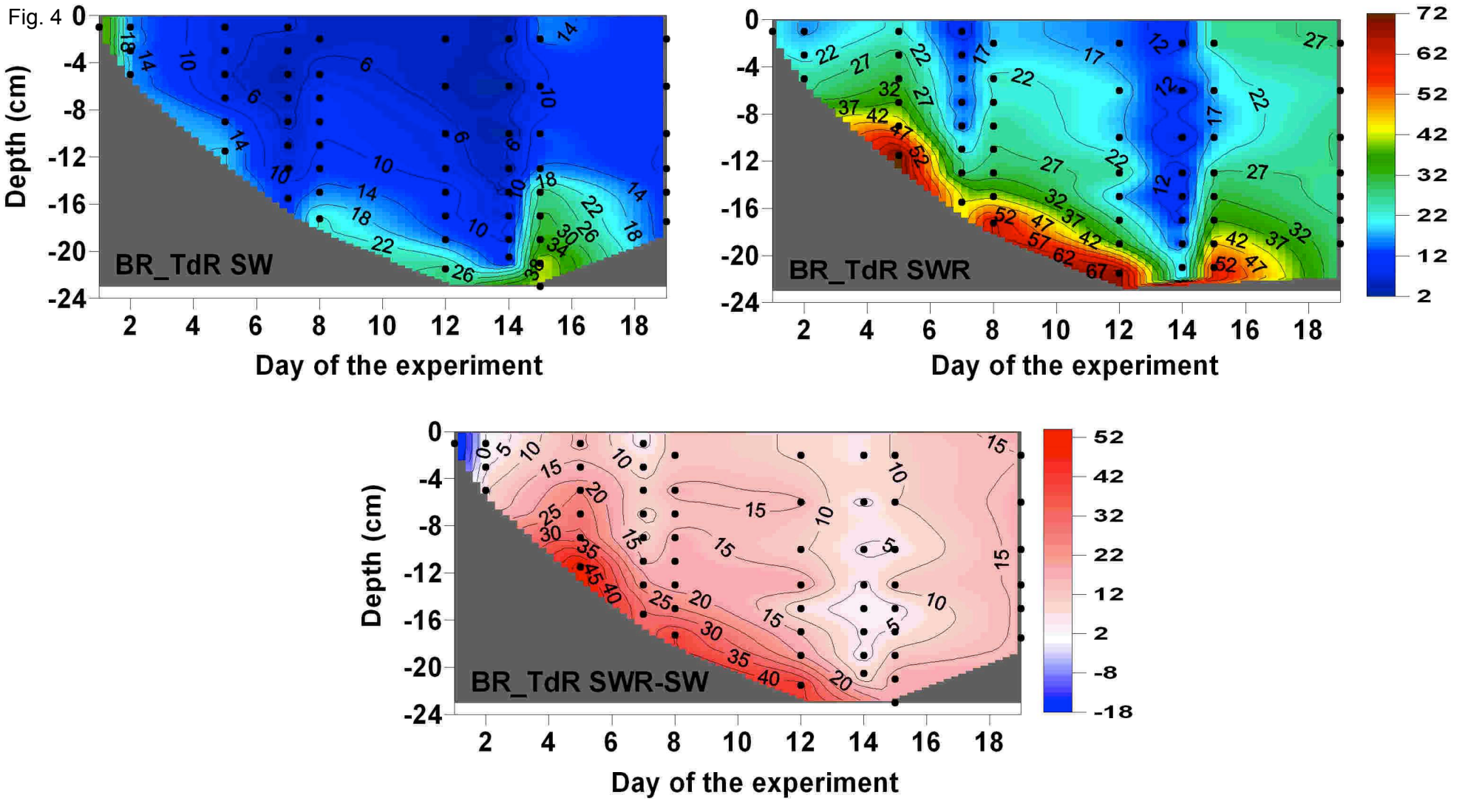
BR_TdR SW
BR_TdR SWR
BR_TdR SWR-SW
Depth (cm)
Day of the experiment
0
-4
-8
-12
-16
-20
-24
2
4
6
8
10
12
14
16
18
72
62
52
42
32
22
12
2
-8
-18

Fig. 5

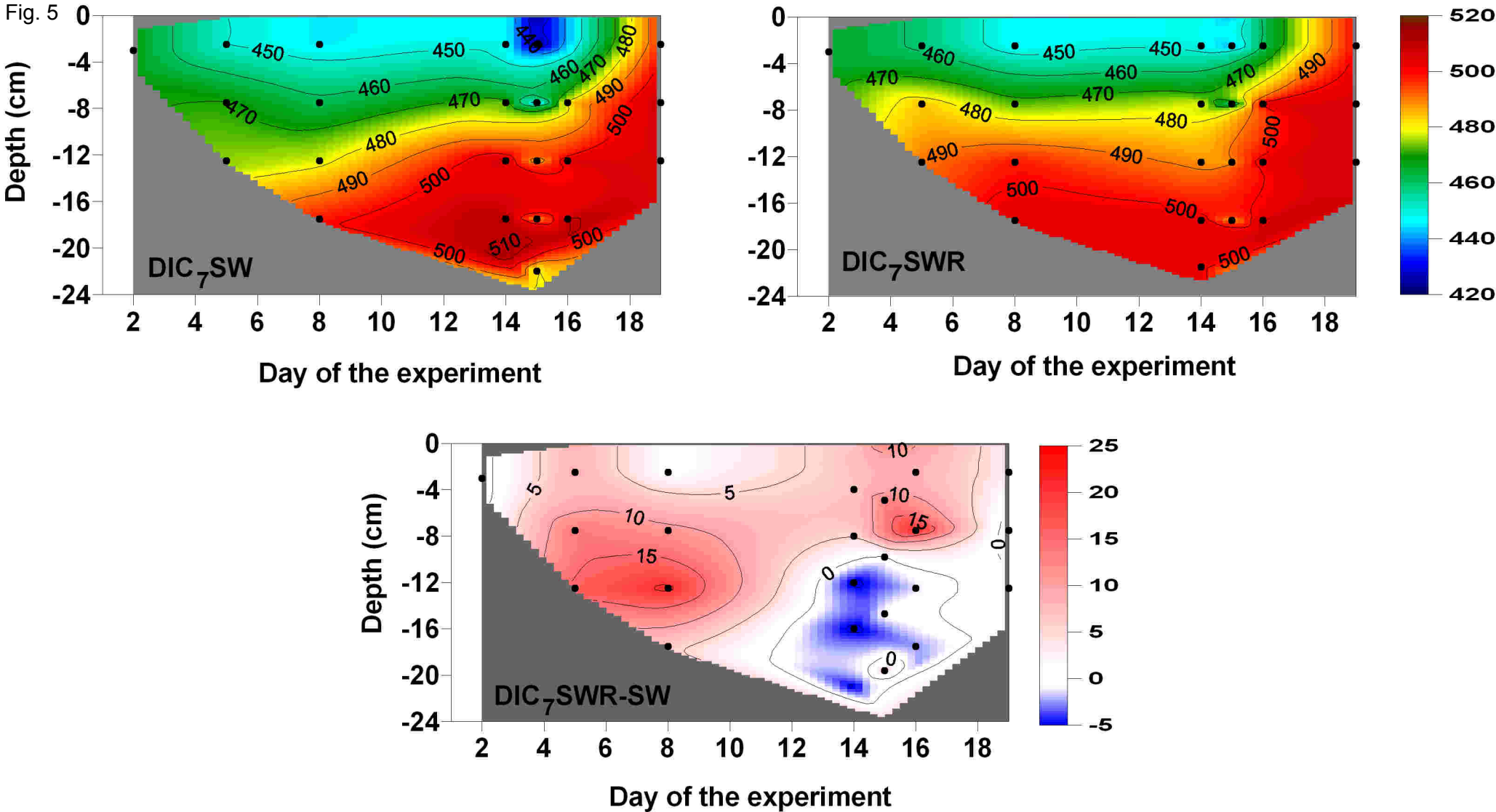
Depth (cm)
0
-4
-8
-12
-16
-20
-24
2
4
6
8
10
12
14
16
18
Day of the experiment
DIC7SW
450
460
470
480
490
500
510
DIC7SWR
520
500
480
460
440
420
DIC7SWR-SW
25
20
15
10
5
0
-5

Fig. 6

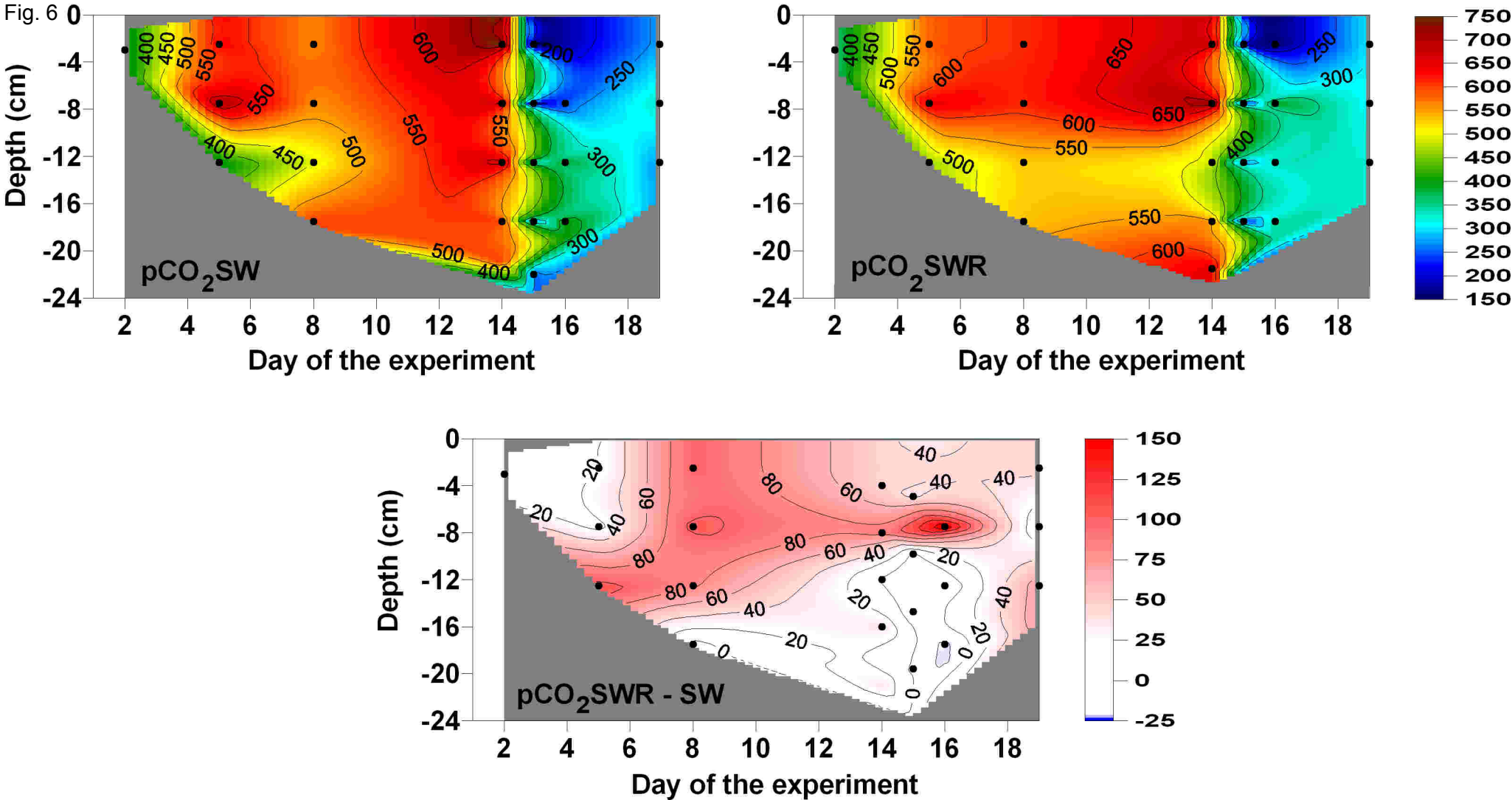
Depth (cm)
0
-4
-8
-12
-16
-20
-24
2
4
6
8
10
12
14
16
18
Day of the experiment
pCO2SW
pCO2SWR
pCO2SWR - SW
750
700
650
600
550
500
450
400
350
300
250
200
150
125
100
75
50
25
0
-25

Fig. 7

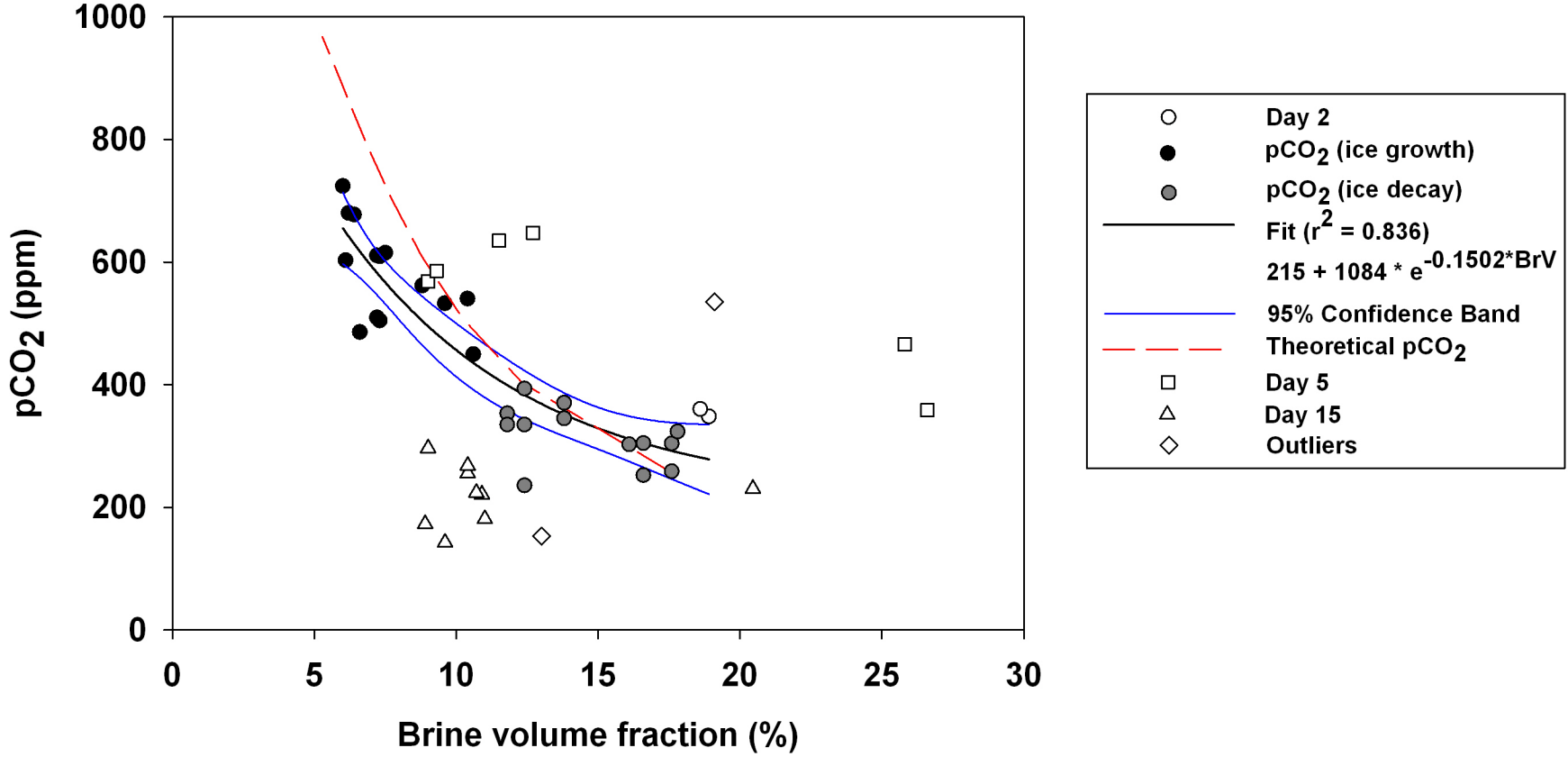
1000
800
600
400
200
0
pCO2 (ppm)
0
5
10
15
20
25
30
Brine volume fraction (%)
Day 2
pCO2 (ice growth)
pCO2 (ice decay)
Fit (r2 = 0.836)
215 + 1084 * e-0.1502*BrV
95% Confidence Band
Theoretical pCO2
Day 5
Day 15
Outliers

Fig. 8

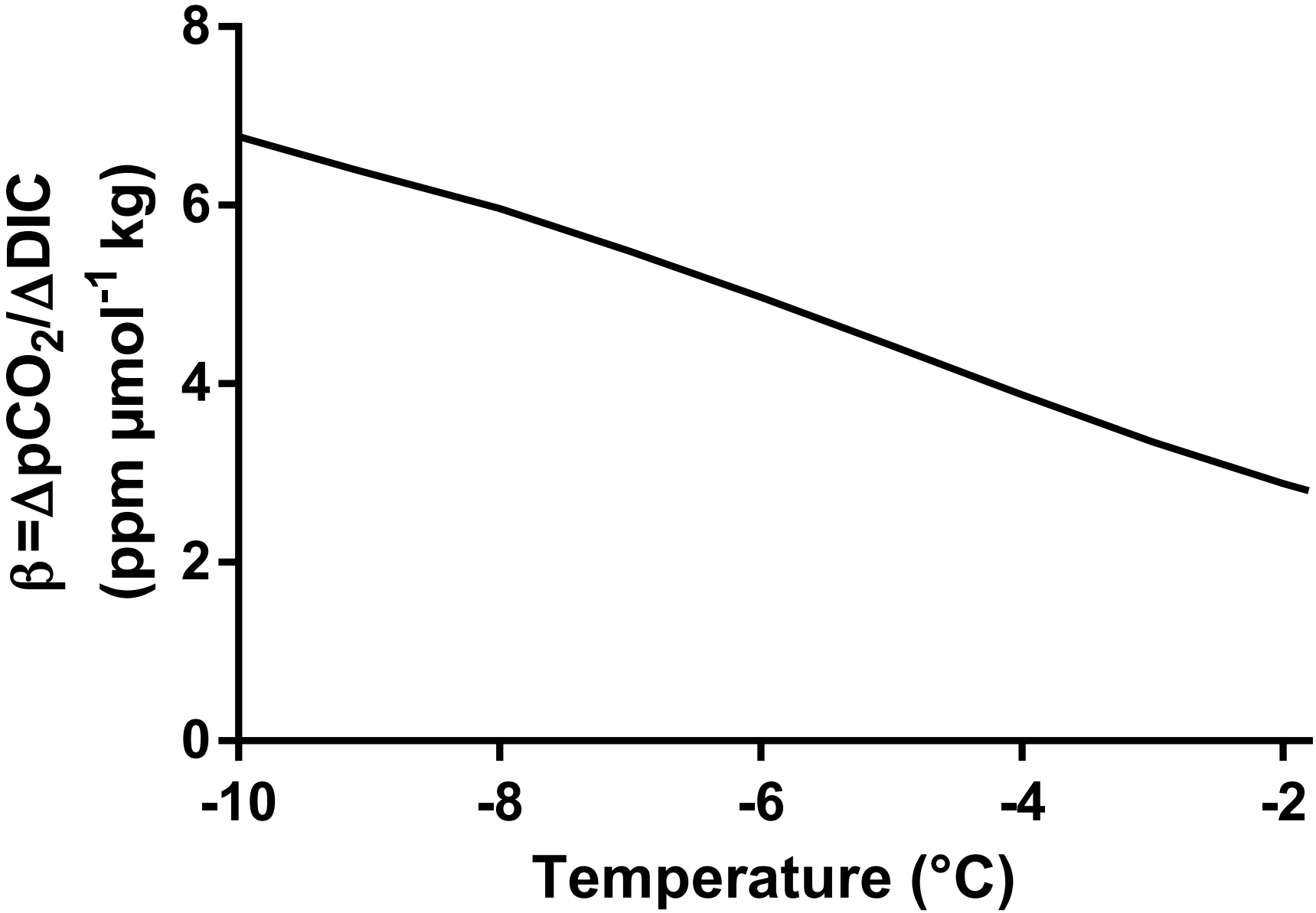

Fig. 9

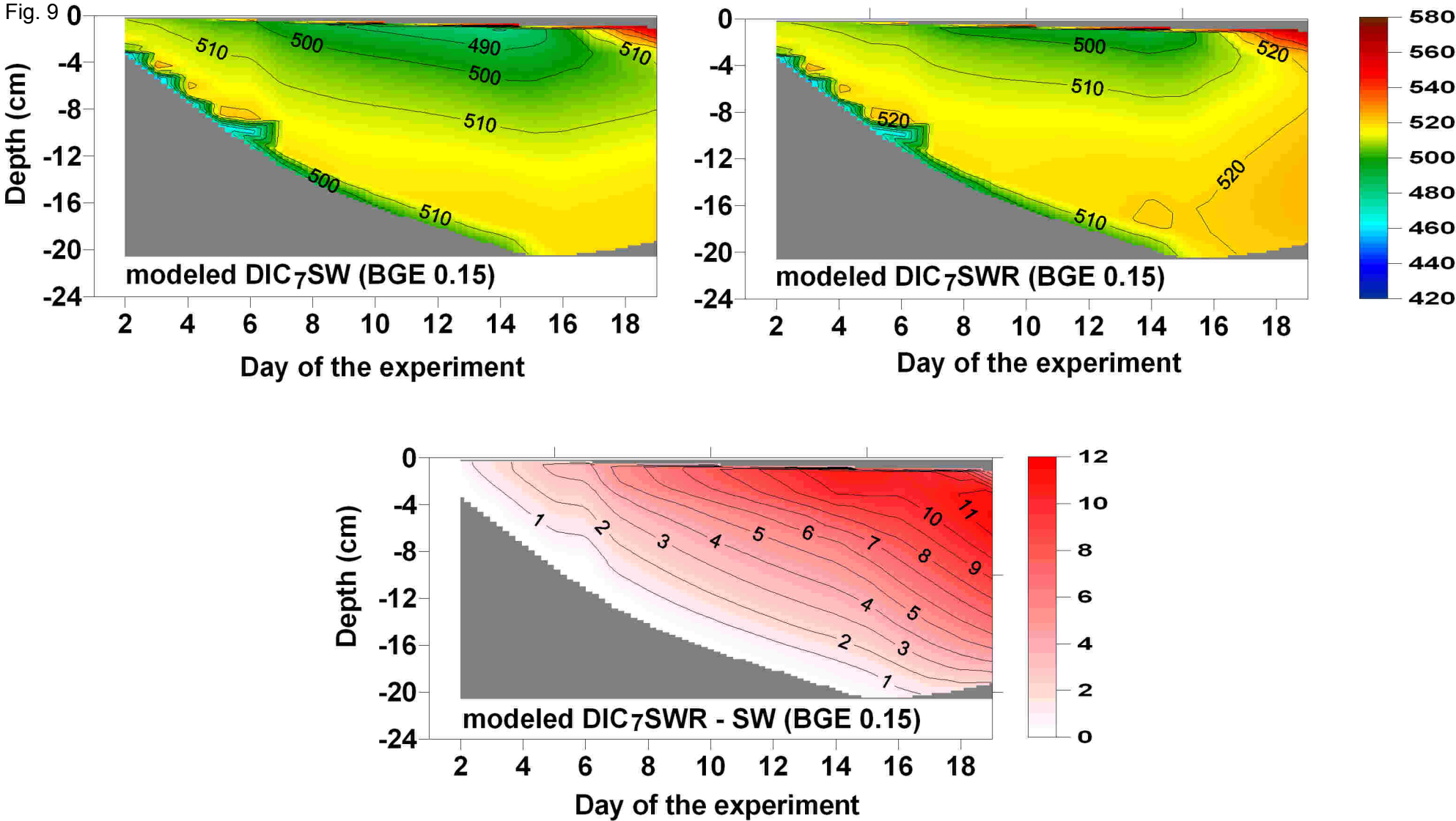
Depth (cm)
0
-4
-8
-12
-16
-20
-24
2
4
6
8
10
12
14
16
18
Day of the experiment
510
500
490
500
510
500
510
modeled DIC7SW (BGE 0.15)
500
510
520
510
520
520
510
modeled DIC7SWR (BGE 0.15)
580
560
540
520
500
480
460
440
420
1
2
3
4
5
6
7
8
9
10
11
4
5
2
3
1
modeled DIC7SWR - SW (BGE 0.15)
12
10
8
6
4
2
0

Fig. 10

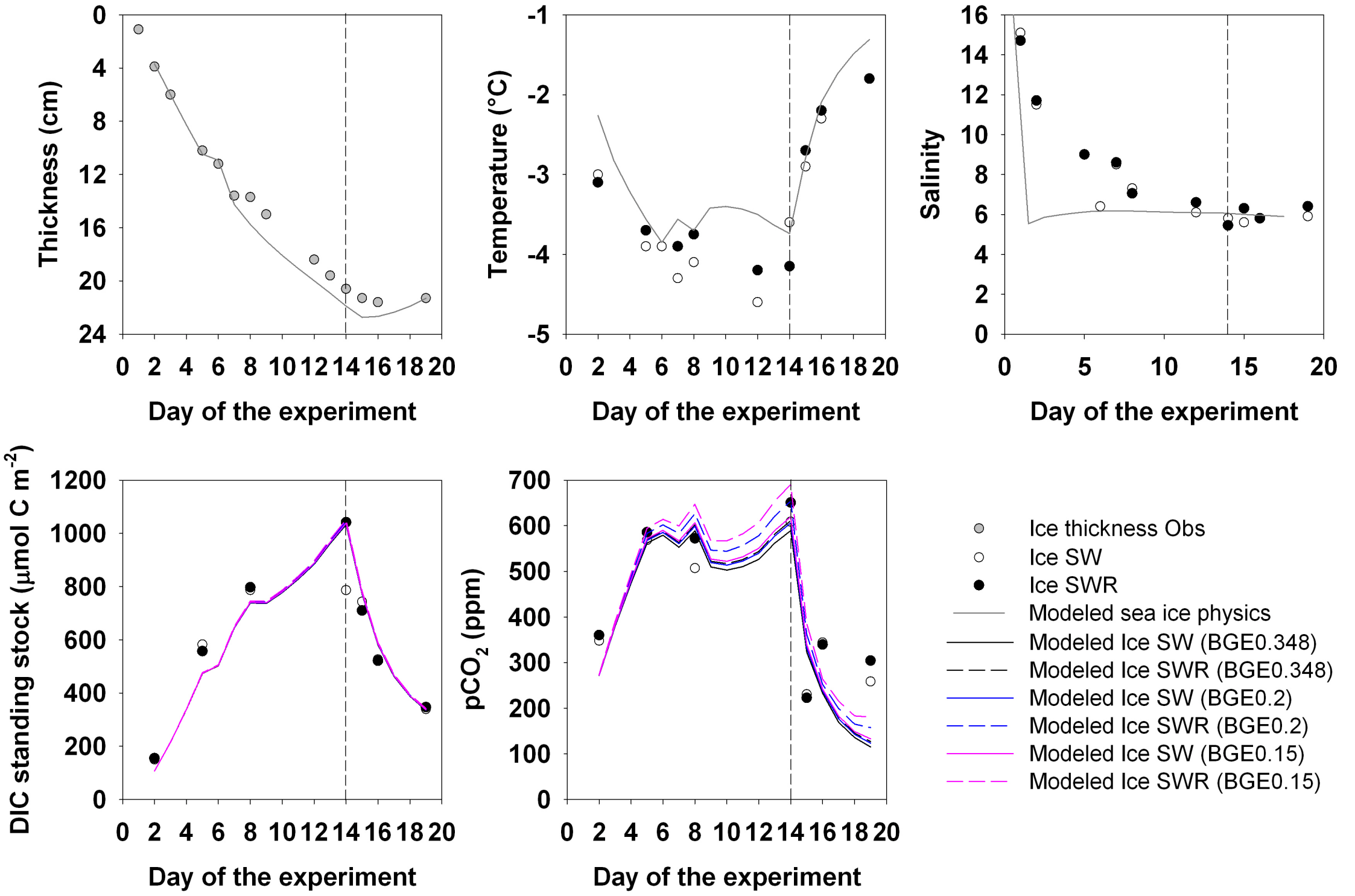
Thickness (cm)
Day of the experiment
Temperature (°C)
Day of the experiment
Salinity
Day of the experiment
DIC standing stock (µmol C m-2)
Day of the experiment
pCO2 (ppm)
Day of the experiment
Ice thickness Obs
Ice SW
Ice SWR
Modeled sea ice physics
Modeled Ice SW (BGE0.348)
Modeled Ice SWR (BGE0.348)
Modeled Ice SW (BGE0.2)
Modeled Ice SWR (BGE0.2)
Modeled Ice SW (BGE0.15)
Modeled Ice SWR (BGE0.15)

Fig. 11

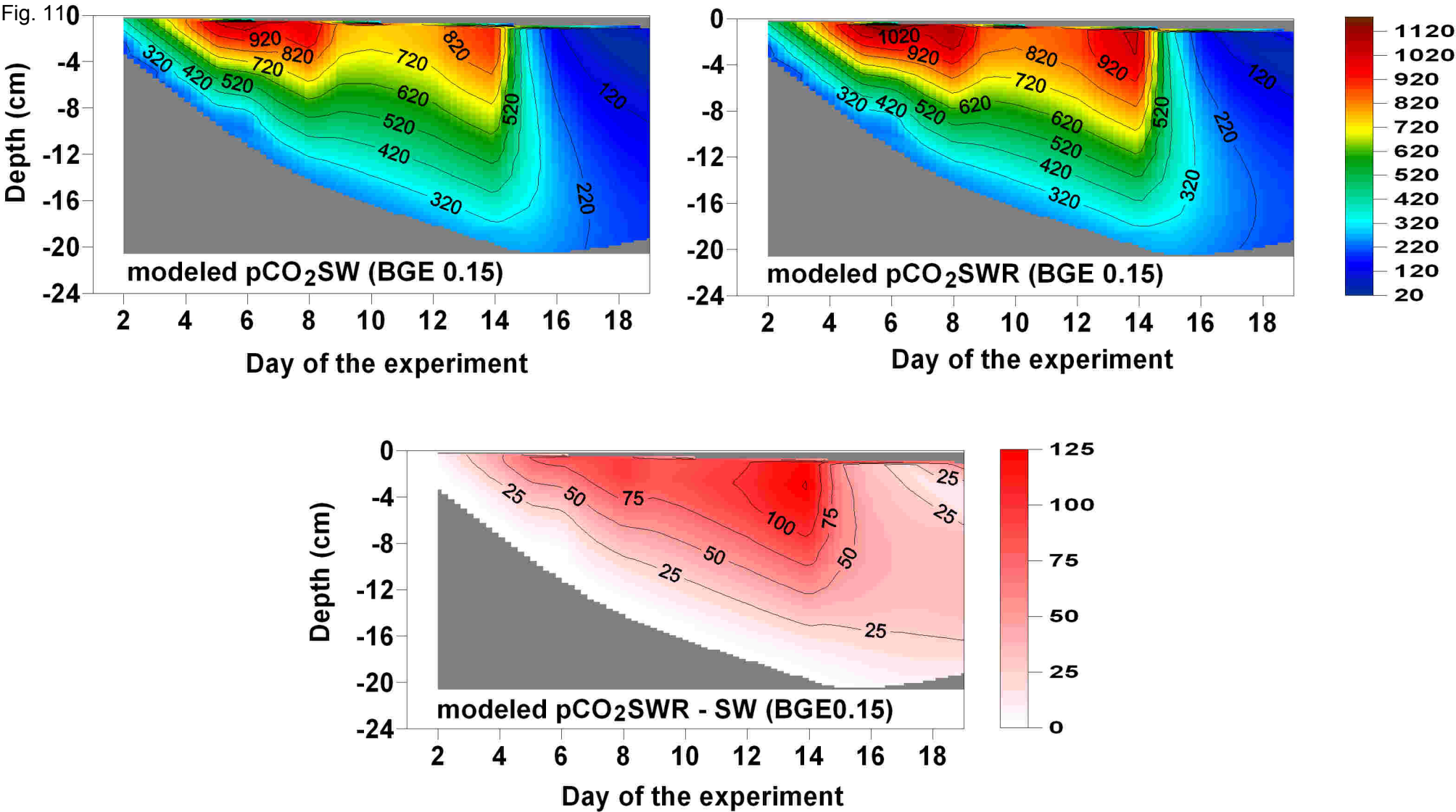
Depth (cm)
0
-4
-8
-12
-16
-20
-24
2
4
6
8
10
12
14
16
18
Day of the experiment
modeled pCO2SW (BGE 0.15)
920
820
720
620
520
420
320
220
120
modeled pCO2SWR (BGE 0.15)
1020
1120
100
75
50
25
modeled pCO2SWR - SW (BGE0.15)
125
0
20